



ELSEVIER

Available online at www.sciencedirect.com

SCIENCE @ DIRECT®

International Journal of Solids and Structures 43 (2006) 144–171

INTERNATIONAL JOURNAL OF
**SOLIDS and
STRUCTURES**

www.elsevier.com/locate/ijsolstr

Extended meshfree analysis of transverse and inplane loading of a laminated anisotropic plate of general planform geometry

Dongdong Wang ^a, Stanley B. Dong ^{b,*}, Jiun-Shyan Chen ^b

^a Department of Civil Engineering, Xiamen University, Xiamen, Fujian 361005, PR China

^b Department of Civil and Environmental Engineering, University of California, P.O. Box 159310, Los Angeles, CA 90095-1593, USA

Received 14 August 2004; received in revised form 25 March 2005

Available online 13 June 2005

Abstract

An extended meshfree method is presented for the analysis of a laminated anisotropic plate under elastostatic loading. The plate may be of any planform shape with its thickness profile composed of perfectly bonded uniform thickness layers of distinct anisotropic materials. Both transverse and inplane loads are considered using a first order shear deformation theory for flexural behavior and generalized plane stress for the membrane behavior. In this extended meshfree method, a rectangular domain is initially considered with the plate of arbitrary geometry inscribed within it. A particular solution in the form of an analytic *generalized Navier* solution (a compound double Fourier series) is used to capture the response due to the loading within the rectangular domain. Then, a homogeneous solution by meshfree analysis is added to treat the augmented boundary conditions on the actual contour of the plate. These augmented conditions are composed of the prescribed values and that of the particular solution evaluated around the plate's contour.

Concentrated transverse and inplane loads in the form of uniform loads over a very small patch are considered with this *generalized Navier* solution representation. When a meshfree portion is added to account for the boundary conditions, such solutions constitute the Green's functions for the plate. The viability of these double Fourier series representations is shown by the convergence rates for the kinematic and force/moment fields. An additional example of a two layer $\pm 30^\circ$ angleply circular plate is given to illustrate the capability of this extended meshfree method.

© 2005 Elsevier Ltd. All rights reserved.

Keywords: Laminated anisotropic plate; Meshfree analysis; *Generalized Navier* solutions; Green's functions

* Corresponding author. Tel.: +1 310 825 5353; fax: +1 310 206 2222.
E-mail address: dong@seas.ucla.edu (S.B. Dong).

1. Introduction

Laminated anisotropic plates have received considerable attention in the last five decades for attributes so universally acknowledged that further elaboration would be superfluous. With respect to structural analysis, Whitney's text (1987), for example, contains a large number of analytical methods for static, free vibration and stability analyses of laminated plates. While it is indeed quite comprehensive, only plates with certain stacking sequences and symmetries and primarily of rectangular planform geometries are treated. An arbitrarily shaped laminated anisotropic plate under general loading will not easily admit an analytical solution.

Herein, we employ an extended meshfree method for the analysis of a laminated anisotropic plate of general planform geometry. In this method, the total response is composed of a particular solution in analytic form for the loading conditions and a meshfree (numerical) homogeneous solution for the boundary conditions. This method for isotropic plates was presented in an earlier paper by the authors, Chen et al. (2004), where the advantages were amply demonstrated. For a general laminated anisotropic plate, there is inherent coupling of extensional and flexural effects. Herein, these inplane and flexural behaviors are represented, respectively, by a generalized plane stress state and by a first order shear deformation theory due to Dong and Chun (1992). The transverse shear rigidities (or alternatively the shear correction factors) are based on a pair of generalized principal shear planes. The concept of generalized principal shear planes is needed because thickness-shear motions in a laminated anisotropic plate may not be polarized in two mutually orthogonal transverse planes. Thickness-shear frequencies at infinitely long wave lengths of this plate theory are made to agree with those of linear three-dimensional elasticity (in the same spirit as Mindlin's theory (1951) for homogeneous, isotropic plates), and this enforcement defines the transverse shear rigidities.

In this version of the extended meshfree method, a rectangular domain is adopted so that the arbitrary plate geometry under consideration can be inscribed within it (see Fig. 1). Analytic solutions for the displacement fields are taken in terms of a pair of generalized double Fourier series over the full rectangular domain, which we dubbed as *generalized Navier* solutions. Two such series are needed, one for transverse load and the other for inplane loads, to accommodate their representations by a double Fourier sine series. Each *generalized Navier* solution by itself will not ordinarily be able to satisfy the boundary conditions, even if the plate is rectangular. The forces, moments and kinematic data around the contour of the plate from these generalized Navier solutions serve as edge loads and constraints to the meshfree plate governing

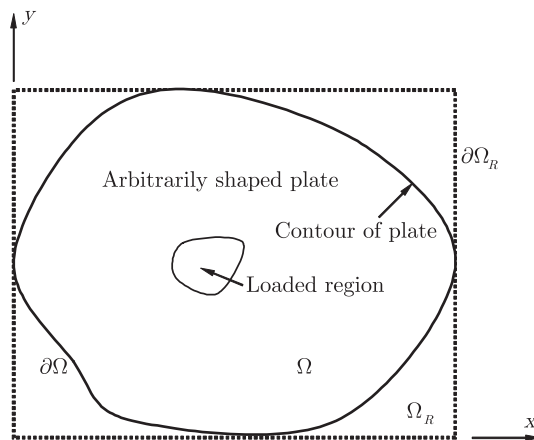


Fig. 1. Diagram of plate inscribed within a rectangular domain.

equations. For the meshfree analysis, a moving least-square/reproducing kernel approximation is used for the kinematic variables, see Belytschko et al. (1994) and Liu et al. (1995). A stabilized conforming nodal integration procedure satisfying linear and bending exactness due to Chen et al. (2001, 2002, 2004) and Wang and Chen (2004) is employed in this formulation. The discretized equations of the weak form are solved subject to prescribed boundary conditions and their modification by the *generalized Navier* solutions. By this extended meshfree method, any shaped plate under arbitrary transverse and inplane loads may be treated.

One important loading condition concerns a concentrated force at some point in the plate. A solution for such a load under given boundary conditions is Green's function. The availability of Green's functions is essential to boundary element and boundary integral equation formulations. The behavior in the vicinity of the load with the extended meshfree method is essentially analytic, which is a significant advantage, especially in comparison to a finite element approach where an ultra fine mesh would be needed. In our examples, we will consider both transverse and inplane concentrated loads, in which each component is represented by a uniform load over an extremely small patch. This substitution of a point source circumvents spurious numerical behavior connected with this singularity. The convergence properties of this patch load representation in the analytic (series) solutions are shown. Once these convergence properties have been quantified, plate responses due to other distributed loading systems are assured of sufficient accuracy as they involve less severe convergence requirements by comparison.

The analyses of inplane and transverse loading of anisotropic plates enjoy a long history beginning with the work of Lekhnitskii in the late 1930s and early 1940s. His text (1957) documents formal solutions to the problems of bending (based on Kirchhoff hypothesis) and inplane loading (via Airy stress function) in terms of analytic functions of two complex variables. Solutions of the same nature were obtained independently by others within this time frame, as Lekhnitskii's publications were not readily available most likely because of WWII. References to these papers may be found in Green and Zerna (1960, p. 185). A resurgence of activity in complex variable solution representations occurred in the early 1990s. Becker in a series of papers (1991, 1992, 1993, 1995) and Zakharov and Becker (2000a,b) presented solutions to laminated anisotropic plates with extension-bending coupling that were based on four complex potential functions. Yin (2003a,b) presented a very complete version of such solutions for extension and bending of laminated anisotropic plates using the Airy stress function and two other stress functions related to the bending and twisting moments. Parallel to these developments were complex variable solution representations based on an extension of Stroh's formalism. Here, we can cite Lu (1994), Lu and Mahrenholtz (1994) and Cheng and Reddy (2002, 2003), who worked on what may be collectively called an octet formalism. Mathematically, these general solution forms are quite elegant and compact. Some specific solutions such as closed form Green's functions for plates of infinite extent have been given, see Becker (1995) and Cheng and Reddy (2003).

While analytical solutions are valuable, their numerical evaluations for stresses and displacements for plates with arbitrary shaped boundaries and general loading conditions pose algebraic challenges. One of the purposes of our present method is to surmount such possible difficulties by means of a combined analytical/numerical solution approach. We believe that such a method will have an appropriate and useful place in the analysis and design of laminated composite plate structures.

2. Governing plate equations

Consider a laminated plate shown in Fig. 1, which is inscribed within a rectangular domain. The plate occupies the region Ω with boundary curve $\partial\Omega$, and the rectangular domain and its perimeter are denoted by Ω_R and $\partial\Omega_R$. Let the x - y plane of a right-handed rectangular Cartesian coordinate system coincide with the middle surface of the plate and let the z -axis be normal to it. Set the origin at the lower left-hand corner of the rectangular domain.

The primary dependent variables in our first order shear deformation theory are the three middle surface displacements and bending rotations ($u, v, w, \theta_x, \theta_y$), eight deformation measures ($\epsilon_{xx}, \epsilon_{yy}, \gamma_{xy}, \gamma_{xz}, \gamma_{yz}, \kappa_{xx}, \kappa_{yy}, \kappa_{xy}$), and the eight force and couple resultants ($N_{xx}, N_{yy}, N_{xy}, Q_x, Q_y, M_{xx}, M_{yy}, M_{xy}$). The sign convention for these quantities is shown in Fig. 2. The deformation measures are interrelated to the kinematic variables by strain–displacement relations.

$$\begin{aligned}
 \epsilon_{xx} &= u_{,x}; & \epsilon_{yy} &= v_{,y}; & \gamma_{xy} &= v_{,x} + u_{,y} \\
 \kappa_{xx} &= \theta_{x,x}; & \kappa_{yy} &= \theta_{y,y}; & 2\kappa_{xy} &= \theta_{y,x} + \theta_{x,y} \\
 \gamma_{xz} &= w_{,x} + \theta_x; & \gamma_{yz} &= w_{,y} + \theta_y
 \end{aligned}
 \tag{1}$$

The constitutive relations for a laminated anisotropic plate can be written in two parts: (1) the extension-bending relations

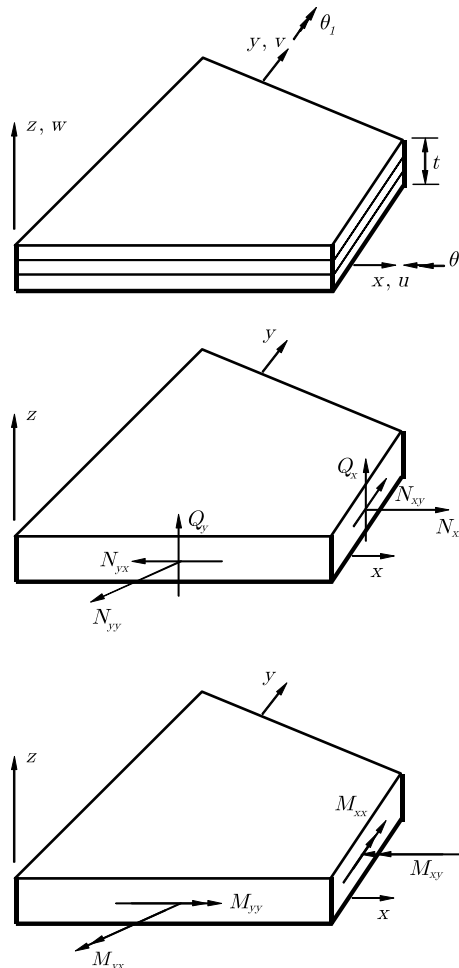


Fig. 2. Element of plate and sign conventions.

$$\begin{Bmatrix} N_{xx} \\ N_{yy} \\ N_{xy} \\ M_{xx} \\ M_{yy} \\ M_{xy} \end{Bmatrix} = \begin{bmatrix} A_{11} & A_{12} & A_{16} & B_{11} & B_{12} & B_{16} \\ A_{12} & A_{22} & A_{26} & B_{12} & B_{22} & B_{26} \\ A_{16} & A_{26} & A_{66} & B_{16} & B_{26} & B_{66} \\ B_{11} & B_{12} & B_{16} & D_{11} & D_{12} & D_{16} \\ B_{12} & B_{22} & B_{26} & D_{12} & D_{22} & D_{26} \\ B_{16} & B_{26} & B_{66} & D_{16} & D_{26} & D_{66} \end{bmatrix} \begin{Bmatrix} \varepsilon_{xx} \\ \varepsilon_{yy} \\ \gamma_{xy} \\ \kappa_{xx} \\ \kappa_{yy} \\ 2\kappa_{xy} \end{Bmatrix} \quad (2)$$

and (2) the transverse shear relations

$$\begin{Bmatrix} Q_x \\ Q_y \end{Bmatrix} = \begin{bmatrix} \Gamma_{55} & \Gamma_{45} \\ \Gamma_{45} & \Gamma_{44} \end{bmatrix} \begin{Bmatrix} \gamma_{xz} \\ \gamma_{yz} \end{Bmatrix} \quad (3)$$

where the A_{ij} , B_{ij} , D_{ij} coefficients are the usual extensional, bending and ext-bend coupling rigidities, whose definitions may be found in any structural composites text, such as [Whitney \(1987\)](#) for example. For the shear rigidities Γ_{55} , Γ_{45} , and Γ_{44} , [Dong and Chun \(1992\)](#) proposed a method for assigning appropriate values to them. Their procedure may be considered as a generalization of [Mindlin's methodology \(1951\)](#) for homogeneous, isotropic plates and that by [Dong and Tso \(1972\)](#) for a first order shear deformation theory for laminated orthotropic constructions.

The equations of equilibrium in rectangular coordinates are

$$\begin{aligned} N_{xx,x} + N_{xy,y} + p_x &= 0 \\ N_{xy,x} + N_{yy,y} + p_y &= 0 \\ Q_{x,x} + Q_{y,y} + q &= 0 \quad \text{in } \Omega \\ M_{xx,x} + M_{xy,y} - Q_x &= 0 \\ M_{xy,x} + M_{yy,y} - Q_y &= 0 \end{aligned} \quad (4)$$

Substituting Eqs. (1)–(3) into Eq. (4) gives displacement equations of equilibrium of the form

$$\begin{bmatrix} L_{11} & L_{12} & 0 & L_{14} & L_{15} \\ L_{12} & L_{22} & 0 & L_{24} & L_{25} \\ 0 & 0 & L_{33} & L_{34} & L_{35} \\ L_{14} & L_{24} & L_{34} & L_{44} & L_{45} \\ L_{15} & L_{25} & L_{35} & L_{45} & L_{55} \end{bmatrix} \begin{Bmatrix} u \\ v \\ w \\ \theta_x \\ \theta_y \end{Bmatrix} = \begin{Bmatrix} -p_x \\ -p_y \\ q \\ 0 \\ 0 \end{Bmatrix} \quad (5)$$

where the operators L_{ij} 's are given in Appendix A. Five boundary conditions may be prescribed on the plate's edge, i.e.,

$$\begin{aligned} u_n &= \bar{u}_n & N_n &= \bar{N}_n \\ u_s &= \bar{u}_s & N_s &= \bar{N}_s \\ \text{either } w &= \bar{w} \text{ or } Q_n &= \bar{Q}_n & \text{ on } \partial\Omega \\ \theta_n &= \bar{\theta}_n & M_{nn} &= \bar{M}_{nn} \\ \theta_s &= \bar{\theta}_s & M_{ns} &= \bar{M}_{ns} \end{aligned} \quad (6)$$

where the overbar denotes a prescribed quantity. This system of governing equations (5) and boundary conditions (6) can be abbreviated as

$$\begin{aligned}\mathcal{L}\mathbf{u} &= \mathbf{f} \quad \text{in } \Omega \\ \mathcal{B}\mathbf{u} &= \mathbf{g} \quad \text{on } \partial\Omega\end{aligned}\tag{7}$$

The weighted residual statement of displacement equations of equilibrium (5), i.e., its weak form, is

$$\begin{aligned}& \int_{\Omega} \int \left\{ \begin{array}{c} \delta\varepsilon \\ \delta\kappa \end{array} \right\}^T \begin{bmatrix} \mathbf{A} & \mathbf{B} \\ \mathbf{B} & \mathbf{D} \end{bmatrix} \left\{ \begin{array}{c} \varepsilon \\ \kappa \end{array} \right\} dA + \int_{\Omega} \int \delta\gamma^T \Gamma \gamma dA \\ &= \int_{\partial\Omega_2} \int (\delta u_n \bar{N}_n + \delta u_s \bar{N}_s + \delta w \bar{Q}_n + \delta \theta_n \bar{M}_{nn} + \delta \theta_s \bar{M}_{ns}) ds + \int_{\Omega} \int (\delta u \bar{p}_x + \delta v \bar{p}_y + \delta w \bar{q}) dA\end{aligned}\tag{8}$$

with $\partial\Omega_2$ as that portion of $\partial\Omega$ where the stress and couple resultants are prescribed and $Q_n \equiv Q_x \cos(\alpha, x) + Q_y \cos(\alpha, y)$ where α is the angle of the unit outward normal with the x -axis.

3. Method of analysis

In the extended meshfree method, the plate under consideration is inscribed within a rectangular region of lateral dimensions (a, b) as shown in Fig. 1. One part of the overall strategy is to use an analytic solution for response to the loading condition, i.e., the particular solution \mathbf{u}_p . But, in constructing \mathbf{u}_p , the rectangular region will be used, so that the particular solution satisfies

$$\mathcal{L}\mathbf{u}_p = \mathbf{f} \quad \text{in } \Omega_R\tag{9}$$

The evaluation of \mathbf{u}_p on the contour $\partial\Omega$ of the plate gives

$$\mathcal{B}\mathbf{u}_p = \mathbf{g}_p \quad \text{on } \partial\Omega\tag{10}$$

which obviously differs from \mathbf{g} . The difference between \mathbf{g}_p and the prescribed boundary conditions \mathbf{g} forms the augmented boundary conditions, which the homogeneous solution must satisfy. Thus, the meshfree analysis for \mathbf{u}_h consists of

$$\begin{aligned}\mathcal{L}\mathbf{u}_h &= \mathbf{0} \quad \text{in } \Omega \\ \mathcal{B}\mathbf{u}_h &= \mathbf{g}_h \quad \text{on } \partial\Omega \text{ where } \mathbf{g}_h = \mathbf{g} - \mathbf{g}_p\end{aligned}\tag{11}$$

For the particular solution, a *generalized Navier* series composed of a pair of double Fourier series is used in the rectangular region. The loading condition must abide by the prescribed distribution within the plate. Outside of the plate, the loading condition is arbitrary and should be taken so as to allow the most convenient double Fourier sine series representation. Since the particular solution is analytic, it will be able to capture the behavior due to the load with as much precision as necessary in accordance with the number of terms used. The convergence of this series solution will be discussed. By means of a Fourier series synthesis, any loading condition can be treated.

By evaluating the *generalized Navier* solution along contour $\partial\Omega$ of the plate, \mathbf{g}_p is found, which will not usually satisfy the prescribed boundary conditions. Thus, the meshfree analysis is concerned with the homogeneous governing differential equations and augmented (nonhomogeneous) boundary conditions composed of the difference between prescribed boundary condition \mathbf{g} and \mathbf{g}_p . The superposition of these analytic and meshfree (numerical) solutions yields a deflection surface satisfying both surface loading conditions and prescribed boundary conditions on the plate's contour. While a finite element analysis can be

employed for these boundary effects, meshfree analysis is eminently more suitable because of its ease in handling continuous boundary data with possibly high spatial variations. By finite elements, boundary loads are treated by consistent loads based on rather elementary interpolation functions used for the stiffness matrices, and fluctuating boundary data will require a commensurately finer mesh for an acceptable accuracy.

4. Generalized Navier solutions

If both transverse and inplane loading conditions are to be represented by double Fourier sine series, then two distinct pairs of double Fourier series are needed as seen in what follows. Consider a rectangular region Ω_R of lateral dimensions (a, b) .

4.1. Transverse loading

For transverse loading, the *generalized Navier* solution form for a plate with the most general form of anisotropy may be taken as

$$\begin{Bmatrix} u \\ v \\ w \\ \theta_x \\ \theta_y \end{Bmatrix} = \sum_{m,n} \begin{Bmatrix} U_{1mn} \sin \alpha_m x \cos \beta_n y + U_{2mn} \cos \alpha_m x \sin \beta_n y \\ V_{1mn} \cos \alpha_m x \sin \beta_n y + V_{2mn} \sin \alpha_m x \cos \beta_n y \\ W_{1mn} \sin \alpha_m x \sin \beta_n y + W_{2mn} \cos \alpha_m x \cos \beta_n y \\ \theta_{x1mn} \cos \alpha_m x \sin \beta_n y + \theta_{x2mn} \sin \alpha_m x \cos \beta_n y \\ \theta_{y1mn} \sin \alpha_m x \cos \beta_n y + \theta_{y2mn} \cos \alpha_m x \sin \beta_n y \end{Bmatrix} \quad (12)$$

where $U_{1mn}, V_{1mn}, W_{1mn}, \dots, \theta_{x2mn}, \theta_{y2mn}$ are the modal amplitudes, α_m, β_n are the wave numbers defined by

$$\alpha_m = \frac{m\pi}{a} \quad \text{and} \quad \beta_n = \frac{n\pi}{b} \quad (13)$$

Accordingly, the transverse loading $q(x, y)$ is represented by a double Fourier sine series.

$$q(x, y) = \sum_m \sum_n q_{mn} \sin \alpha_m x \sin \beta_n y \quad (14)$$

Substitution of Eqs. (12) and (14) into governing equation (9) gives ten equations for the ten unknown modal amplitudes $U_{1mn}, V_{1mn}, W_{1mn}, \dots, \theta_{x2mn}, \theta_{y2mn}$ in terms of q_{mn} for each pair of wave numbers (m, n) . These equations are given in Appendix A. The inplane strains, changes of curvature and transverse shear angles based on this solution form can be calculated in a straight-forward manner, and these series expressions may also be found in Appendix A.

For rectangular plates with certain laminate profiles, for example a cross-ply layup, only one series in Eq. (12) is needed as all of the coefficients in the other series are identically zero. In this case, freely supported conditions exist for the transverse behavior and mixed boundary conditions hold for inplane behavior on $\partial\Omega_R$. But for a plate with the most general form of anisotropy and laminate construction, the complete form of Eq. (12) is needed. The full series is doubly periodic in both coordinate directions, but it portrays no meaningful boundary conditions on the rectangle's contour $\partial\Omega_R$.

4.2. Inplane loading

In an analogous manner, the *generalized Navier* solution form for inplane loading is taken as

$$\begin{pmatrix} u \\ v \\ w \\ \theta_x \\ \theta_y \end{pmatrix} = \sum_{m,n} \begin{pmatrix} U_{3mn} \sin \alpha_m x \sin \beta_n y + U_{4mn} \cos \alpha_m x \cos \beta_n y \\ V_{3mn} \cos \alpha_m x \cos \beta_n y + V_{4mn} \sin \alpha_m x \sin \beta_n y \\ W_{3mn} \sin \alpha_m x \cos \beta_n y + W_{4mn} \cos \alpha_m x \sin \beta_n y \\ \theta_{x3mn} \cos \alpha_m x \cos \beta_n y + \theta_{x4mn} \sin \alpha_m x \sin \beta_n y \\ \theta_{y3mn} \sin \alpha_m x \sin \beta_n y + \theta_{y4mn} \cos \alpha_m x \cos \beta_n y \end{pmatrix} \quad (15)$$

where $U_{3mn}, V_{3mn}, W_{3mn}, \dots, \theta_{x4mn}, \theta_{y4mn}$ are the modal amplitudes. This double Fourier series form enables the expansion of inplane loads as a double Fourier sine series.

$$p_x(x, y) = \sum_m \sum_n p_{xmn} \sin \alpha_m x \sin \beta_n y; \quad p_y(x, y) = \sum_m \sum_n p_{ymn} \sin \alpha_m x \sin \beta_n y \quad (16)$$

Substitution of solution form (15) and loading conditions (16) into governing equations (9) gives another set of ten equations for the unknown modal amplitudes $U_{3mn}, V_{3mn}, W_{3mn}, \dots, \theta_{x4mn}, \theta_{y4mn}$ in terms of p_{xmn} and p_{ymn} for each set of wave numbers (m, n) . The system of ten algebraic equations and the equations for the inplane strains, etc. may be found in Appendix A. This second set of equations is virtually identical to the first set except for a certain number of signs. Similar remarks regarding realistic boundary conditions on the rectangular contour $\partial\Omega_R$ can be made.

5. Meshfree plate equations

In the meshfree method of analysis, a set of NP nodes (x_I, y_I) , $I = 1, 2, \dots, NP$ is used in the domain Ω occupied by the plate. The plate's kinematic behavior is represented by approximations over these discrete points. Herein, a moving least-square/reproducing kernel approximation is used for the kinematic variables as summarized in the next section. Then we set forth the approximations of the kinematic variables and their deformation measures and discuss the integration procedure used in this meshfree formulation to generate the discrete equations of equilibrium. These equations evince linear and bending exactness as well as lock free shear behavior.

5.1. Moving least-square/reproducing kernel (MLSRK) approximation

For the plate domain containing NP discretized nodes (x_I, y_I) , the moving least-square/reproducing kernel approximation of a field variable $f(x, y)$, denoted by $f^h(x, y)$, is expressed by

$$f^h(x, y) = \sum_{I=1}^{NP} \Psi_I(x, y) d_I \quad (17)$$

where d_I is the nodal coordinate and shape function $\Psi_I(x, y)$ is given by

$$\Psi_I(x, y) = \mathbf{H}^T(x - x_I, y - y_I) \mathbf{b}(x, y) \phi(x - x_I, y - y_I) \quad (18)$$

with $\phi(x - x_I, y - y_I)$ as the kernel function centered at (x_I, y_I) with a compact support, and \mathbf{H}^T and \mathbf{b} are vectors, respectively, of an n th order monomial basis and its associated coefficients, i.e.,

$$\begin{aligned} \mathbf{H}^T(x - x_I, y - y_I) &= \{1, x - x_I, y - y_I, \dots, (x - x_I)^n, \dots, (y - y_I)^n\}^T \\ \mathbf{b}(x, y) &= \{b_{00}(x, y), b_{10}(x, y), b_{01}(x, y), \dots, b_{n0}(x, y), \dots, b_{0n}(x, y)\}^T \end{aligned} \quad (19)$$

The b_{ij} coefficients are determined by imposing the following n th order reproducing conditions

$$\sum_{I=1}^{NP} \Psi_I(x, y) x_I^i y_I^j = x^i y^j, \quad 0 \leq i + j \leq n \quad (20)$$

which is equivalent to

$$\sum_{I=1}^{NP} \Psi_I(x, y) (x - x_I)^i (y - y_I)^j = \delta_{i0} \delta_{j0}, \quad 0 \leq i + j \leq n \quad (21)$$

or

$$\sum_{I=1}^{NP} \Psi_I(x, y) \mathbf{H}(x - x_I, y - y_I) = \mathbf{H}(0, 0)$$

where δ_{ij} is the Kronecker delta. Substituting Eq. (18) into Eq. (21) and solving for b_{ij} yields the shape functions as

$$\Psi_I(x, y) = \mathbf{H}^T(0, 0) \mathcal{M}^{-1}(x, y) \mathbf{H}(x - x_I, y - y_I) \phi(x - x_I, y - y_I) \quad (22)$$

with \mathcal{M} is a moment matrix given by

$$\mathcal{M}(x, y) = \sum_{I=1}^{NP} \mathbf{H}(x - x_I, y - y_I) \mathbf{H}^T(x - x_I, y - y_I) \phi(x - x_I, y - y_I) \quad (23)$$

This MLS/RK approximation is valid for any order n . Herein, a second order basis is used, i.e., $n = 2$.

5.2. Approximation of the kinematic and deformation fields

By the MLS/RK approximation procedure, the vectorial form of the approximated kinematic variables at the nodes in terms of shape functions $\Psi_I(x, y)$ is

$$\mathbf{u}^h(x, y) = \begin{Bmatrix} u^h \\ v^h \\ w^h \\ \theta_x^h \\ \theta_y^h \end{Bmatrix} = \sum_{I=1}^{NP} \Psi_I(x, y) \begin{Bmatrix} u_I \\ v_I \\ w_I \\ \theta_{xI} \\ \theta_{yI} \end{Bmatrix} \equiv \sum_{I=1}^{NP} \Psi_I(x, y) \mathbf{d}_I \quad (24)$$

where superscript h connotes an approximation of the exact field. The deformation measures of Eq. (1) then take on the following forms

$$\begin{Bmatrix} \varepsilon^h(x, y) \\ \kappa^h(x, y) \end{Bmatrix} = \begin{Bmatrix} \varepsilon_{xx}^h \\ \varepsilon_{yy}^h \\ \gamma_{xy}^h \\ \kappa_{xx}^h \\ \kappa_{yy}^h \\ 2\kappa_{xy}^h \end{Bmatrix} = \sum_{I=1}^{NP} \mathbf{B}_I^b(x, y) \mathbf{d}_I \quad (25)$$

$$\gamma^h(x, y) = \begin{Bmatrix} \gamma_{xz}^h \\ \gamma_{yz}^h \end{Bmatrix} = \sum_{I=1}^{NP} \mathbf{B}_I^s(x, y) \mathbf{d}_I \quad (26)$$

where

$$\mathbf{B}_I^b(x, y) = \begin{bmatrix} \Psi_{I,x} & 0 & 0 & 0 & 0 \\ 0 & \Psi_{I,y} & 0 & 0 & 0 \\ \Psi_{I,y} & \Psi_{I,x} & 0 & 0 & 0 \\ 0 & 0 & 0 & \Psi_{I,x} & 0 \\ 0 & 0 & 0 & 0 & \Psi_{I,y} \\ 0 & 0 & 0 & \Psi_{I,y} & \Psi_{I,x} \end{bmatrix} \quad (27)$$

$$\mathbf{B}_I^s(x, y) = \begin{bmatrix} 0 & 0 & \Psi_{I,x} & \Psi_I & 0 \\ 0 & 0 & \Psi_{I,y} & 0 & \Psi_I \end{bmatrix} \quad (28)$$

5.3. Smoothed kinematic measures

These deformation measures are to be incorporated into the weak form statement of the governing equations and must be integrated over the domain occupied by the plate. In this integration process, a stabilized conforming nodal integration procedure is needed to avoid numerical instabilities and to satisfy the so-called linear and bending exactness, i.e., the patch tests. This is achieved by introducing the following deformation smoothing of the middle surface strains and curvatures at node (x_K, y_K) , see Wang and Chen (2004).

$$\tilde{\varepsilon}^h(x_K, y_K) \frac{1}{A_K} \iint_{A_K} \begin{Bmatrix} u_x(x, y) \\ v_y(x, y) \\ u_y(x, y) + v_x(x, y) \end{Bmatrix} dA \quad (29)$$

$$\tilde{\kappa}^h(x_K, y_K) \frac{1}{A_K} \iint_{A_K} \begin{Bmatrix} \theta_x(x, y) \\ \theta_y(x, y) \\ \theta_y(x, y) + \theta_x(x, y) \end{Bmatrix} dA \quad (30)$$

where the tildes connote approximation and A_K is the nodal representative area that can be obtained, for example, from a Voronoi diagram, see Fig. 3. To satisfy the (integration) constraints of Eqs. (29) and (30), invoke the divergence theorem to convert the area integrals to line integrals around the representative area A_K , i.e.,

$$\begin{aligned} \tilde{\varepsilon}_{xx}^h(x_K, y_K) &= \frac{1}{A_K} \iint_{A_K} u_x(x, y) dA = \oint_{S_K} u n_x ds \\ \tilde{\gamma}_{xy}^h(x_K, y_K) &= \frac{1}{A_K} \iint_{A_K} \{u_y(x, y) + v_x(x, y)\} dA = \oint_{S_K} \{u n_y + v n_x\} ds \\ \tilde{\kappa}_{xx}^h(x_K, y_K) &= \frac{1}{A_K} \iint_{A_K} \theta_{x,x}(x, y) dA = \oint_{S_K} \theta_x n_x ds \\ 2\tilde{\kappa}_{xy}^h(x_K, y_K) &= \frac{1}{A_K} \iint_{A_K} \{\theta_{x,y}(x, y) + \theta_{y,x}(x, y)\} dA = \oint_{S_K} \{\theta_x n_y + \theta_y n_x\} ds \end{aligned} \quad (31)$$

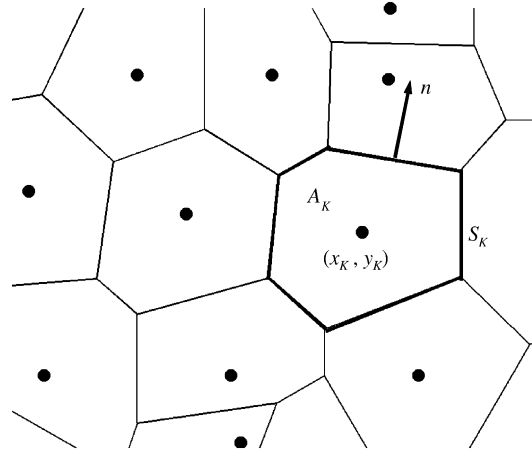


Fig. 3. Nodal representative area (Voronoi diagram).

where S_K is the close boundary of the representative area A_K and n_x, n_y are the components of the unit outward normal \mathbf{n} as shown in Fig. 3. Hence, the inplane strains and bending curvatures of Eqs. (29) and (30) become

$$\tilde{\mathbf{B}}_I^b(x, y) = \begin{bmatrix} \tilde{\nabla}_x \Psi_I & 0 & 0 & 0 & 0 \\ 0 & \tilde{\nabla}_y \Psi_I & 0 & 0 & 0 \\ \tilde{\nabla}_y \Psi_I & \tilde{\nabla}_x \Psi_I & 0 & 0 & 0 \\ 0 & 0 & 0 & \tilde{\nabla}_x \Psi_I & 0 \\ 0 & 0 & 0 & 0 & \tilde{\nabla}_y \Psi_I \\ 0 & 0 & 0 & \tilde{\nabla}_y \Psi_I & \tilde{\nabla}_x \Psi_I \end{bmatrix} \quad (32)$$

where $\tilde{\nabla}_\alpha$ is the smoothed gradient notation given by

$$\tilde{\nabla}_\alpha \Psi_I(x_K, y_K) = \oint_{S_K} \Psi_I(x, y) n_\alpha(x, y) ds \alpha = (x, y) \quad (33)$$

5.4. Discretized equations

Incorporating the smoothed inplane strains and bending curvatures into the nodally integrated weak form given by Eq. (7) at (x_K, y_K) gives

$$\begin{aligned} & \sum_{K=1}^{NP} \left\{ \left\{ \begin{array}{l} \delta \tilde{\mathbf{e}}(x_K, y_K) \\ \delta \tilde{\mathbf{k}}(x_K, y_K) \end{array} \right\}^T \begin{bmatrix} \mathbf{A} & \mathbf{B} \\ \mathbf{B} & \mathbf{D} \end{bmatrix} \left\{ \begin{array}{l} \tilde{\mathbf{e}}(x_K, y_K) \\ \tilde{\mathbf{k}}(x_K, y_K) \end{array} \right\} + \delta \gamma^T(x_K, y_K) \Gamma \gamma(x_K, y_K) \right\} A_K \\ &= \sum_{L=1}^{NS} \left\{ \delta u(x_L, y_L) \bar{N}_{xx}(x_L, y_L) + \delta v(x_L, y_L) \bar{N}_{yy}(x_L, y_L) + \delta w(x_L, y_L) \bar{Q}_n(x_L, y_L) + \delta \theta_x(x_L, y_L) \bar{M}_{xx} \right. \\ & \quad \left. + \delta \theta_y(x_L, y_L) \bar{M}_{yy} \right\} \tilde{w}_L + \sum_{K=1}^{NP} \left\{ \delta u(x_K, y_K) \bar{p}_x(x_K, y_K) + \delta v(x_K, y_K) \bar{p}_y(x_K, y_K) + \delta w(x_K, y_K) \bar{q}(x_K, y_K) \right\} A_K \end{aligned} \quad (34)$$

where (x_L, y_L) and \tilde{w}_L are the sampling point and weight, respectively, of the numerical integration procedure for the boundary integral, which is assumed to be taken over NS points whose supports intersect with the plate's contour. Evaluation of this equation leads to the discrete equations as

$$\mathbf{Kd} = [\mathbf{K}^b + \mathbf{K}^s]\mathbf{d} = \mathbf{f}^S + \mathbf{f}^A \tag{35}$$

where $\mathbf{K}^b, \mathbf{K}^s, \mathbf{f}^S, \mathbf{f}^A$ are the assembled nodal stiffnesses and load vectors, respectively,

$$\mathbf{K}^b = \mathcal{A}_{I,J=1}^{NP} \mathbf{K}_{IJ}^b; \quad \mathbf{K}^s = \mathcal{A}_{I,J=1}^{NP} \mathbf{K}_{IJ}^s; \quad \mathbf{f}^S = \mathcal{A}_{I=1}^{NS} \mathbf{f}_I^S; \quad \mathbf{f}^A = \mathcal{A}_{I=1}^{NP} \mathbf{f}_I^A \tag{36}$$

where \mathcal{A} denotes an assembly operation and submatrices of \mathbf{K}_{IJ}^b and \mathbf{K}_{IJ}^s are given by

$$\mathbf{K}_{IJ}^b = \sum_{K=1}^{NP} \mathbf{B}_I^{bT}(x_K, y_K) \begin{bmatrix} \mathbf{A} & \mathbf{B} \\ \mathbf{B} & \mathbf{D} \end{bmatrix}_{6 \times 6} \mathbf{B}_I^b(x_K, y_K) A_K, \tag{37}$$

$$\mathbf{K}_{IJ}^s = \sum_{K=1}^{NP} \mathbf{B}_I^{sT}(x_K, y_K) \Gamma_{2 \times 2} \mathbf{B}_I^s(x_K, y_K) A_K \tag{38}$$

and

$$\mathbf{f}_I^S = \sum_{L=1}^{NS} \Psi_I(x_L, y_L) \left\{ \begin{array}{l} \bar{N}_{xx}(x_L, y_L) \\ \bar{N}_{yy}(x_L, y_L) \\ \bar{Q}_n(x_L, y_L) \\ \bar{M}_x(x_L, y_L) \\ \bar{M}_y(x_L, y_L) \end{array} \right\} \tilde{w}_L \quad \text{and} \quad \mathbf{f}_I^A = \sum_{K=1}^{NP} \Psi_I(x_K, y_K) \left\{ \begin{array}{l} \bar{p}_x(x_K, y_K) \\ \bar{p}_y(x_K, y_K) \\ \bar{q}(x_K, y_K) \\ 0 \\ 0 \end{array} \right\} A_K \tag{39}$$

The system of Eq. (35) is capable of treating a laminated anisotropic plate of arbitrary geometry under general loading conditions. However, in this extended meshfree version, only \mathbf{f}^S representing boundary kinematic measures and loads is involved as surface loads are treated by the particular solution. In this system of equations, both linear/bending exactness and lock free shear behavior are satisfied due to the treatment of inplane and flexural deformations by our stabilized nodal integration method. This system of equations represents the extension of the authors' previous paper, i.e., [Chen et al. \(2004\)](#), applied to homogeneous, isotropic plates where bending exactness and lock free shear behavior were demonstrated.

6. Point loads/Green's functions

For convenience in our discussion of concentrated transverse and inplane loads, consider a rectangular plate of sides (a, b) loaded by forces, (P_x, P_y, P_z) , at location $(x = \xi, y = \eta)$. The double Fourier series of Eqs. (14) and (16) for these load components are

$$\{p_x, p_y, q\}(x, y; \xi, \eta) = \frac{4}{ab} \{P_x, P_y, P_z\} \sum_m \sum_n \sin \alpha_m \xi \sin \beta_n \eta \sin \alpha_m x \sin \beta_n y \tag{40}$$

Since these expansions do not converge, a more relaxed representation consisting of uniform loads (p_{x0}, p_{y0}, p_{z0}) over a extremely small rectangular patch of dimensions (R, S) is substituted for these concentrated forces. The coefficients $(p_{xmn}, p_{ymn}, q_{mn})$ in the double Fourier series representations for these loads are

$$\{p_{xmn}, p_{ymn}, q_{mn}\} = \frac{16\{p_{x0}, p_{y0}, q_0\}}{ab\alpha_m\beta_n} \sin \alpha_m \xi \sin \beta_n \eta \sin \frac{\alpha_m R}{2} \sin \frac{\beta_n S}{2} \tag{41}$$

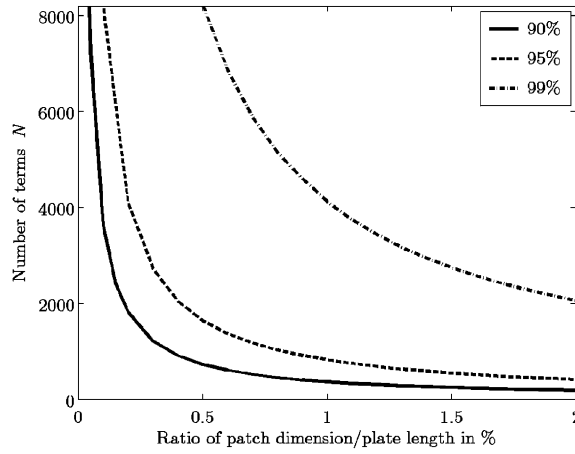


Fig. 4. Number of terms vs patch dimension/plate length ratio for equivalent point load.

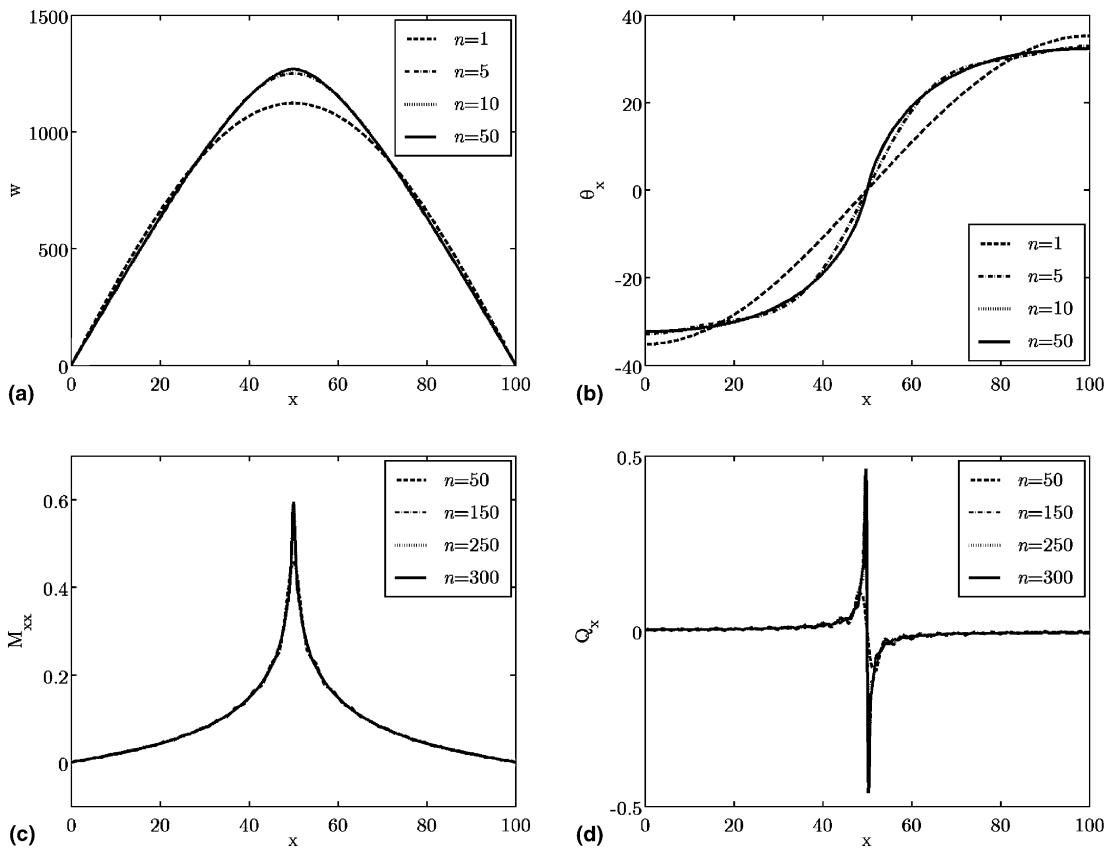


Fig. 5. Rectangular isotropic plate—unit transverse load at center: Plots of (a) $w(x, 50)$, (b) $\theta_x(x, 50)$, (c) $M_{xx}(x, 50)$ and (d) $Q_x(x, 50)$.

The equivalence to concentrated forces of these magnitudes is measured by

$$\int_{\xi-R/2}^{\xi+R/2} \int_{\eta-S/2}^{\eta+S/2} \{p_{x0}, p_{y0}, q_0\} dx dy = \{P_x, P_y, P_z\} \quad \text{or} \quad \{p_{x0}, p_{y0}, q_0\} = \frac{\{P_x, P_y, P_z\}}{RS} \quad (42)$$

While a doubly infinite number of terms are needed for full equivalence, convergence on a practical basis can be measured by the number of terms according to patch size to achieve a particular percentage of the total load (say, 90%, 95% and 99%). The plot in Fig. 4 shows the number of terms N for a given percentage of the total load versus patch size as expressed by the ratio of patch width to plate length. Since the loaded region is rectangular, the total number of terms would be N^2 . While Fig. 4 indicates a discouraging low convergence rate for a 99% equivalence, our plate results in the examples that follow show that significantly

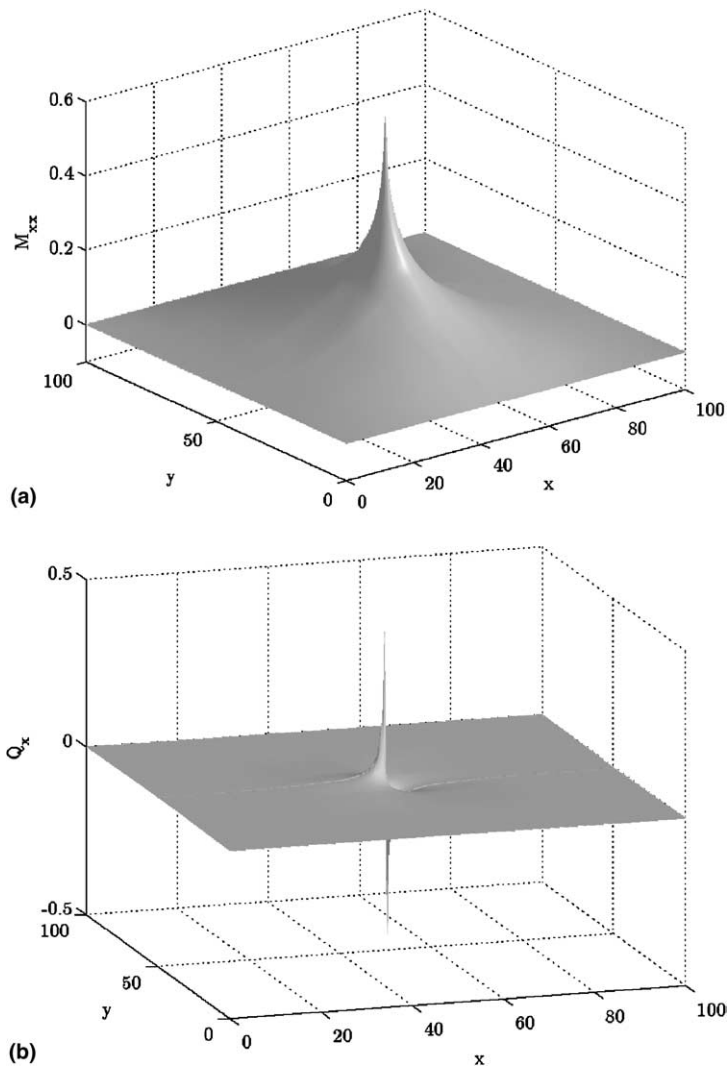


Fig. 6. Rectangular isotropic plate—unit transverse load at center: Three-dimensional plots of (a) M_{xx} and (b) Q_x fields.

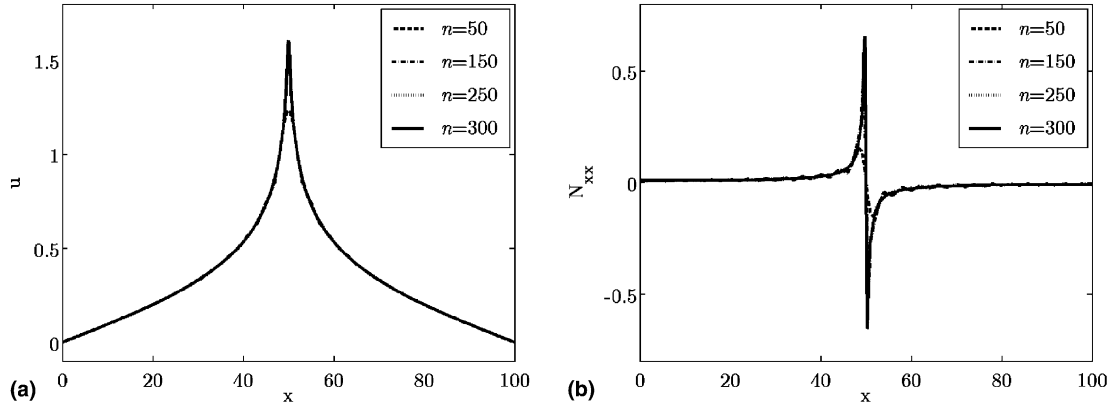


Fig. 7. Rectangular isotropic plate—unit longitudinal load in x -direction at center: plots of (a) $u(x, 50)$ and (b) $N_{xx}(x, 50)$.

fewer terms are sufficient for accurate results, even for near singular force and moment fields associated with the concentrated forces due to the inherent nature of the *generalized Navier* series.

Two square plates are considered in this section: an isotropic plate and a two-layer $\pm 30^\circ$ angleply plate both of side dimension $a = 100$ and thickness/length ratio $h/a = 1/100$. For the isotropic plate, Poisson's ratio $\nu = 0.3$. For the two-layer $\pm 30^\circ$ angleply plate, the material properties parallel and perpendicular to the fiber direction are

$$\frac{E_L}{E_T} = 40; \quad \frac{G_{LT}}{E_T} = 0.5; \quad \frac{G_{TT}}{E_T} = 0.2; \quad \nu_{LT} = 0.25; \quad \nu_{TT} = 0.25 \quad (43)$$

Unit transverse and inplane concentrated forces at the center of the plate are considered, where a square patch of width equal to 0.5% of a , i.e., $R/a = S/a = 0.005$, is used for them. The isotropic plate results are normalized with respect to Young's modulus E , and those for the two-layer angleply plate by E_T .

6.1. Homogeneous isotropic plate

For a unit transverse load, a family of plots of displacement w , slope θ_x , moment M_{xx} and transverse shear Q_x along a line through the middle of the plate is shown in Fig. 5, i.e., on a line between end points $(x, y) = (0, 50)$ and $(100, 50)$. The number of terms in the Fourier series are indicated in the family of curves. It is seen that the kinematic field was captured with a very few terms; $N = 10$ in most cases were sufficient for four significant digit accuracy, while $N = 5$ gave reasonably acceptable results. On the other hand, the moment and transverse shear force fields required substantially more terms since they involve near singular behavior.¹ Nevertheless, the numbers of terms are substantially less than that to capture the equivalent load as shown in Fig. 4. Three-dimensional plots of the near singular moment M_{xx} and shear Q_x fields are shown in Fig. 6.

For the inplane unit load, near singular behavior is seen in both u and N_{xx} in Fig. 7. The inplane force N_{xx} which is proportional to the derivative of u is clearly correlated in the two plots of Fig. 7. Moreover, the numbers of terms needed for accurate results are similar those for M_{xx} and Q_x for transverse loading.

¹ In the computational procedure, the Fourier coefficients of the kinematic field are determined once, and all subsequent calculations of force and moment data involve summations of these coefficients. For a desk top computer with a Pentium 4 microprocessor, these summations required a matter of seconds to generate the data for these plots.

Although no three-dimensional plots of near singular behavior of inplane loading results are presented for this loading condition, such plots would evince the same near singular behavior as the flexural field. From common understanding of finite element modeling, it is obvious that an extremely fine mesh would be needed for such results.

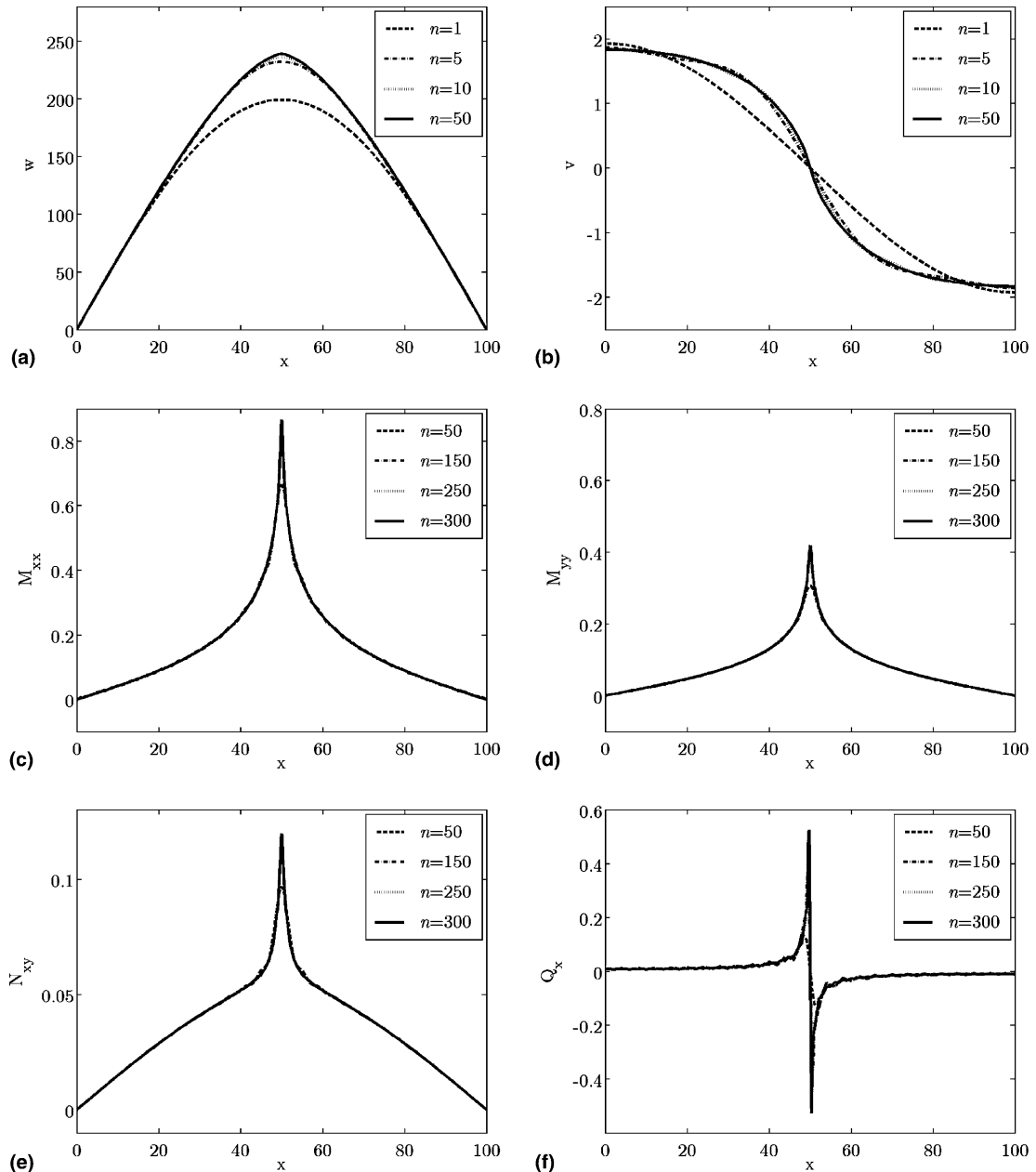


Fig. 8. Rectangular two-layer $\pm 30^\circ$ angleply plate—unit transverse load at center: plots of (a) $w(x, 50)$, (b) $v(x, 50)$, (c) $M_{xx}(x, 50)$, (d) $M_{yy}(x, 50)$, (e) $N_{xy}(x, 50)$ and (f) $Q_x(x, 50)$.

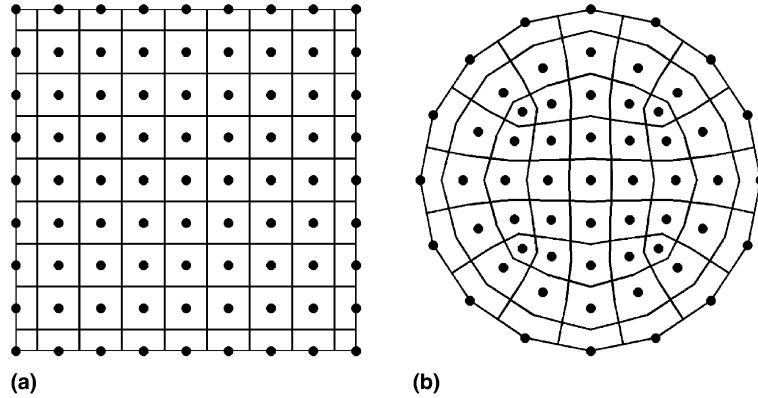


Fig. 9. Meshfree layouts of rectangular and circular plate geometries.

For an isotropic plate, only one series in Eq. (12) or (15) is involved; thus the boundary conditions along the perimeter $\partial\Omega_R$ are those of a freely supported condition for transverse loading and mixed boundary conditions for inplane loading. For any other condition, a meshfree analysis must be added. For example, if the edge were clamped, a normal moment distribution around the perimeter must be applied. Since the governing differential equations of equilibrium are elliptic-like, such applied edge moments will decay rapidly into the interior of the plate. Because a meshfree analysis of this isotropic plate will reveal little in terms of new behavior, such an analysis will not be presented here for brevity sake.

6.2. Square two-layer $\pm 30^\circ$ angleply plate

For a square two layer $\pm 30^\circ$ angleply plate of side dimension a , the properties of Eq. (43) in a two-layer plate with layer thickness equal to half of the total depth, the values of \mathbf{A} , \mathbf{B} , \mathbf{D} and Γ^2 are

$$\mathbf{A} = \begin{bmatrix} 23.0667 & 7.4810 & 0.0 \\ & 3.5362 & 0.0 \\ \text{sym.} & & 7.7306 \end{bmatrix}; \quad \mathbf{B} = \begin{bmatrix} 0.0 & 0.0 & 3.1579 \\ & 0.0 & 1.0706 \\ \text{sym.} & & 0.0 \end{bmatrix} \quad (44)$$

$$\mathbf{D} = \begin{bmatrix} 1.9222 & 0.6234 & 0.0 \\ & 0.2947 & 0.0 \\ \text{sym.} & & 0.6442 \end{bmatrix}; \quad \Gamma = \begin{bmatrix} 0.2817 & 0.0 \\ 0.0 & 0.1896 \end{bmatrix}$$

For this layup of the two plies, B_{16} and B_{26} are present. Thus, coupling between inplane forces (N_{xx}, N_{yy}) and twisting moment M_{xy} , as well as between normal bending moments (M_{xx}, M_{yy}) and inplane shear N_{xy} will be seen.

For a unit transverse load, plots of displacements (w, v) and of moments and forces M_{xx} , M_{yy} , N_{xy} , and Q_x along a line through the middle of the plate connecting end points $(x, y) = (0, 50)$ and $(100, 50)$ are shown in Fig. 8. Again, the number of terms in the *generalized Navier* series are shown to indicate the convergence of these fields. These plots show convergence rates that are very much like those for the isotropic plate. As cited in the Introduction, there are a number of classical theory solutions for a point load for a laminated

² See Dong and Chun (1992).

anisotropic plate of infinite extent. No comparisons of the accuracy of these analytic point load solutions were made with the current numerical results, since the latter data are based on a first order shear deformation plate theory. The singular solutions in the literature are appropriate for an accompanying homogeneous solution predicated on classical theory.

If this angleply plate were fully clamped on all four sides so that all displacement and normal bending rotations are suppressed, then a meshfree homogeneous solution must be added where a normalized

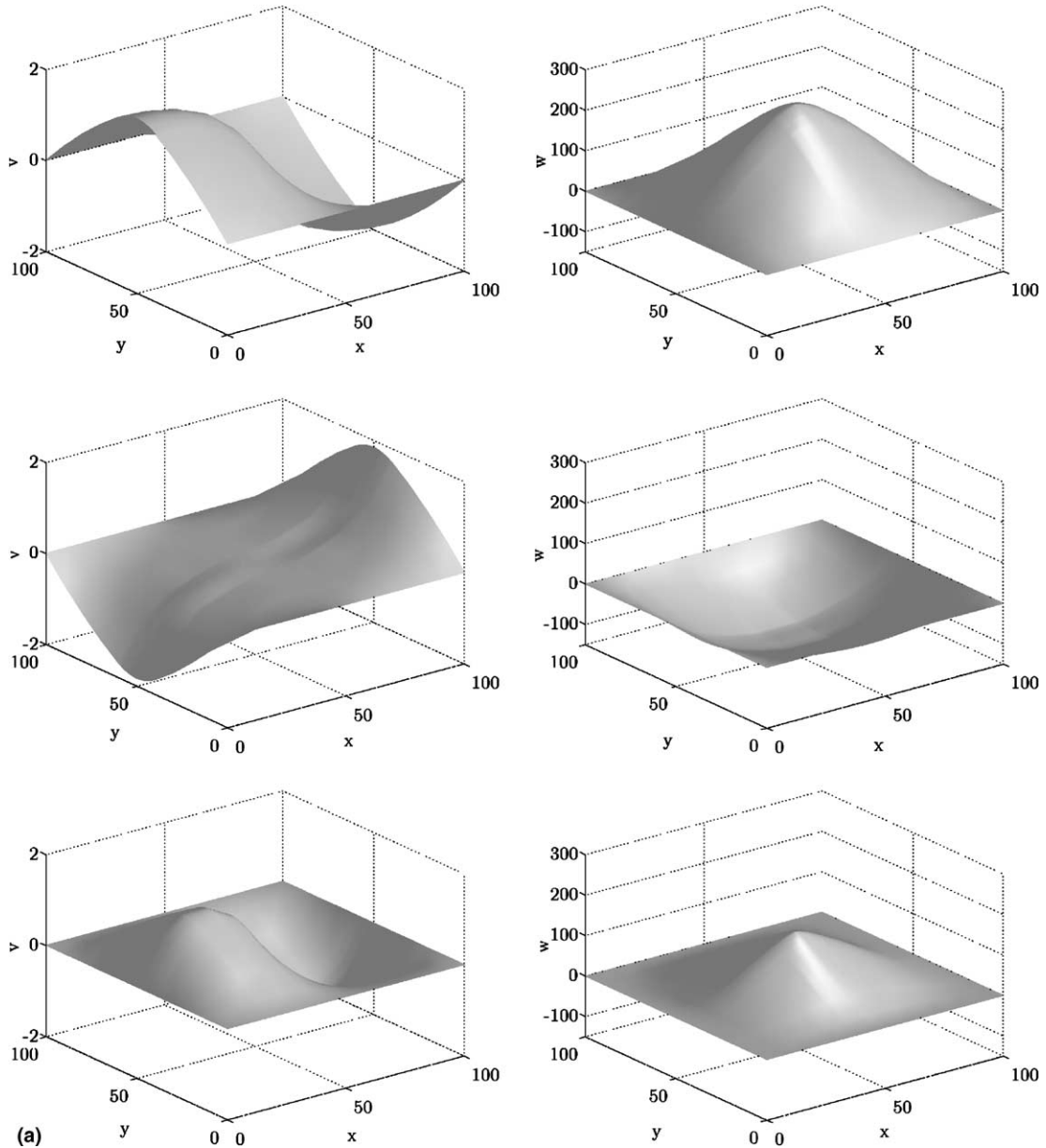


Fig. 10. (a) Rectangular two-layer $\pm 30^\circ$ angleply plate—unit transverse load at center: three-dimensional plots of (a) v and (b) w fields.

support size of 2.5 was used. The layout of points for the meshfree analysis of this square plate is shown in Fig. 9(a). The particular, homogeneous and total solutions are shown in Fig. 10, where Fig. 10(a) contains the displacement fields v and w , Fig. 10(b) the slope θ_x and moment M_{xx} , and Fig. 10(c) the forces Q_x and N_{xy} . In these figures, those in the first row depict the particular solution, the second row contains the homogeneous solution and the bottom row gives the total solution. The response to the near concentrated force over the entire plate is clearly visualized in these three-dimensional figures.

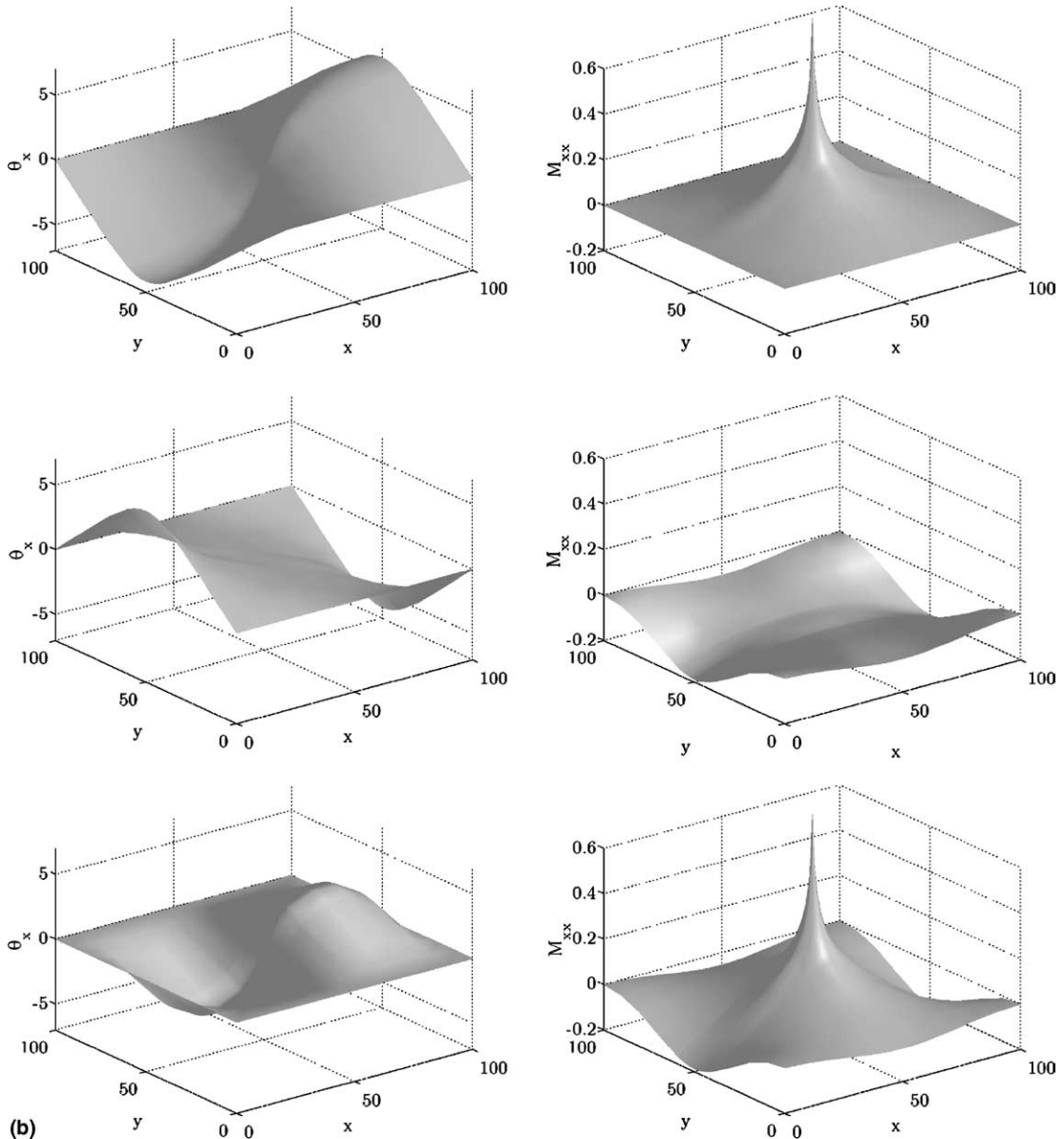


Fig. 10. (b) Rectangular two-layer $\pm 30^\circ$ angleply plate—unit transverse load at center: three-dimensional plots of (a) θ_x and (b) M_{xx} fields.

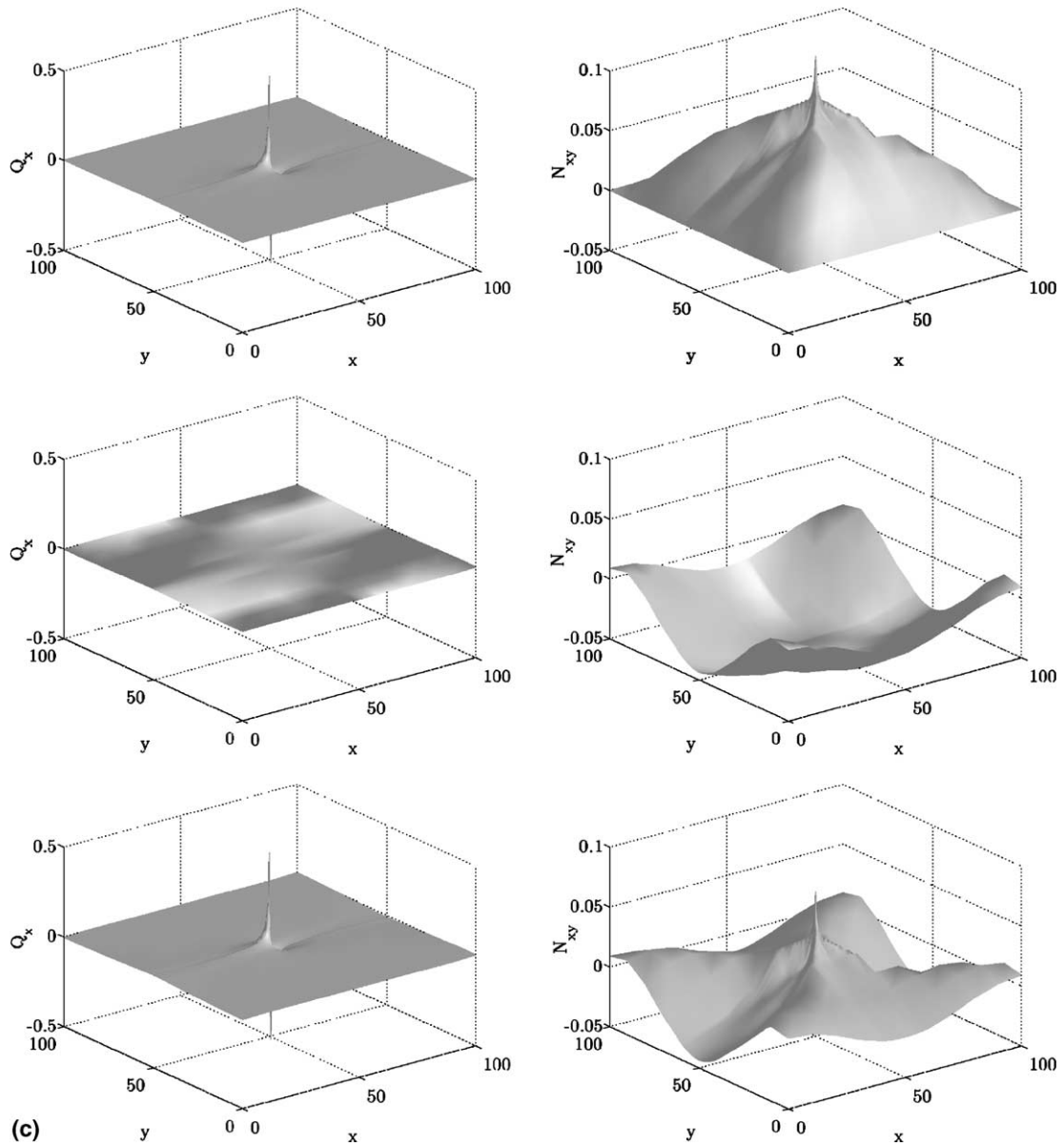


Fig. 10. (c) Rectangular two-layer $\pm 30^\circ$ angleply plate—unit transverse load at center: three-dimensional plots of (a) Q_x and (b) N_{xy} fields.

For a unit inplane load represented by uniformly distributed load over a same size patch of $R/a = S/a = 0.005$, the results for u , θ_y , N_{xx} and Q_y along a line through the middle of the plate connecting end points $(x, y) = (0, 50)$ and $(100, 50)$ are shown in Fig. 11. The convergence rates for this loading condition evince the same trends as the isotropic plate. A three-dimensional plot of Q_y is shown in Fig. 12, where the reversal of the sign of Q_y was made for a clearer visualization. As the homogeneous solution will be very similar in nature to that for the transverse loading condition, no meshfree analysis is presented here.

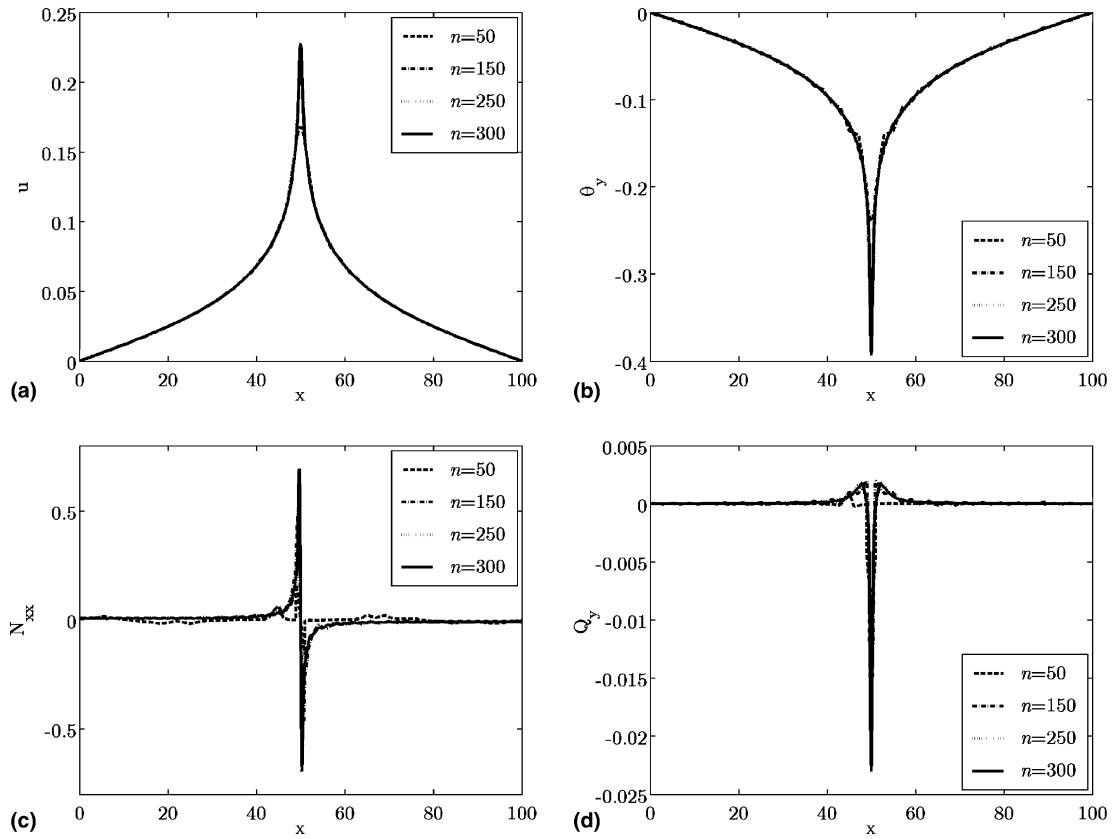


Fig. 11. Rectangular two-layer $\pm 30^\circ$ angleply plate—unit longitudinal load in x -direction at center: Plots of (a) $u(x, 50)$, (b) $\theta_y(x, 50)$, (c) $N_{xx}(x, 50)$ and (d) $Q_y(x, 50)$.

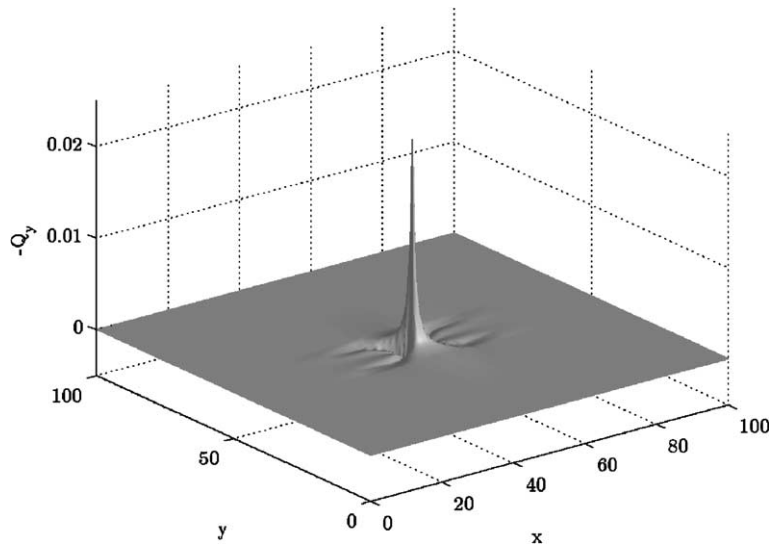


Fig. 12. Rectangular two-layer $\pm 30^\circ$ angleply plate—unit longitudinal load in x -direction at center: three-dimensional plot of Q_y field.

7. Circular two-layer $\pm 30^\circ$ angleply plate with an off center load

Consider a circular two layer $\pm 30^\circ$ angleply plate with a radius of 50 units. Let the $\pm 30^\circ$ ply angles be oriented with respect to the x -axis. A unit concentrated transverse force occurs on a 45° radial line with the center of the plate at a distance of $20\sqrt{2}$ units away from it. This load is represented by using a square pad

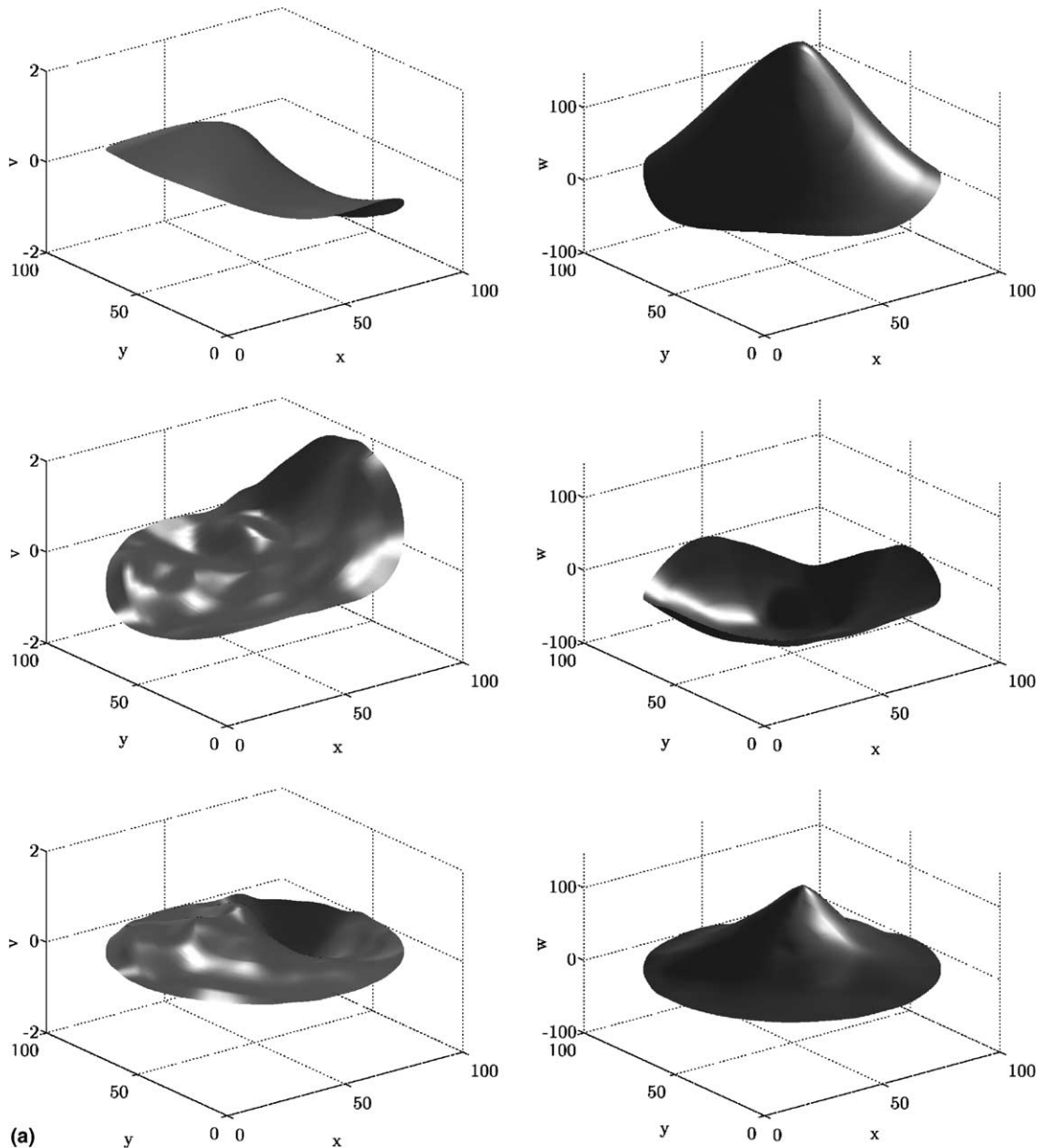


Fig. 13. (a) Circular two-layer $\pm 30^\circ$ angleply plate—unit transverse load at $(\zeta, \eta) = (70, 70)$: three-dimensional plots of (a) v and (b) w fields.

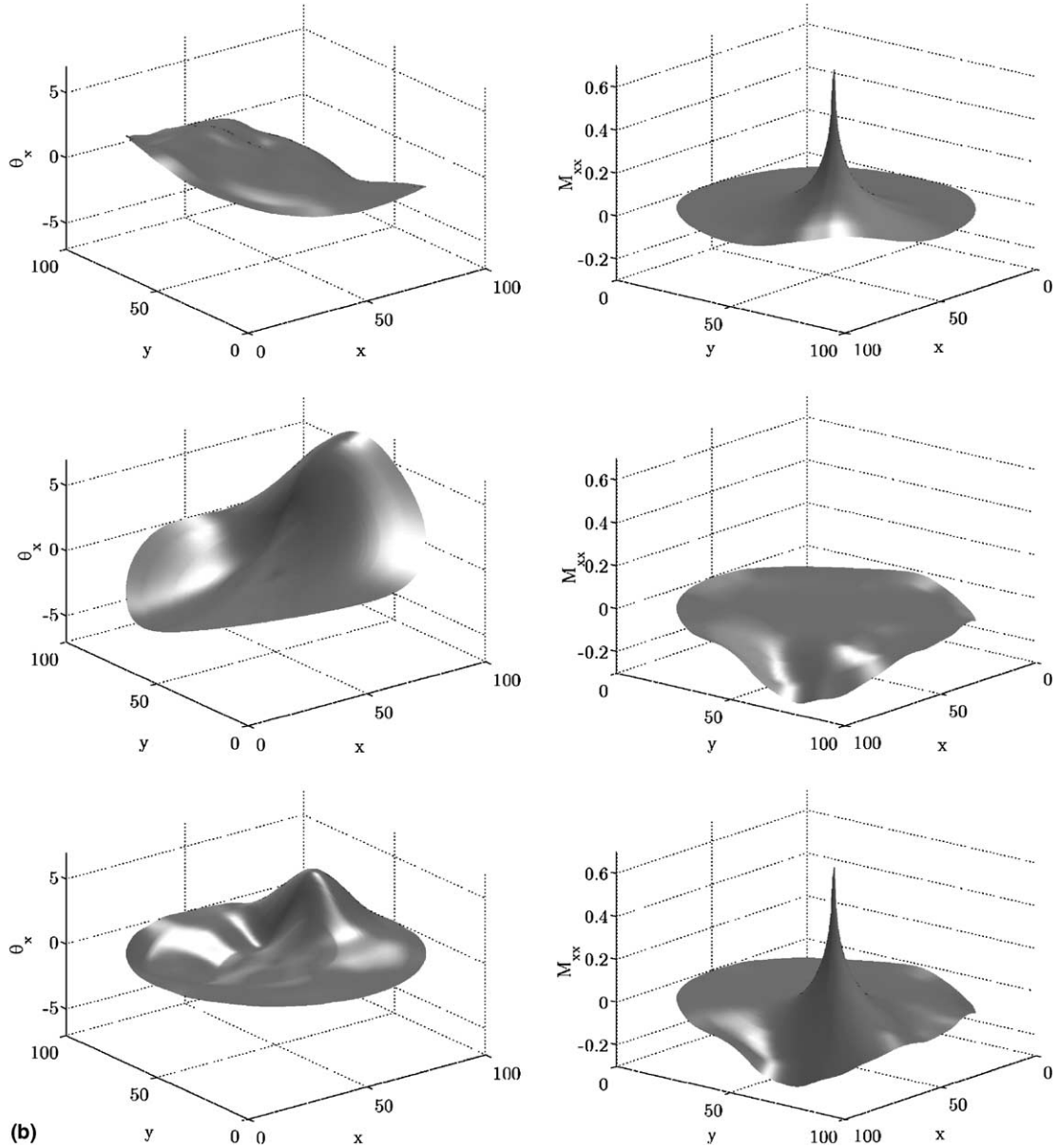


Fig. 13. (b) Circular two-layer $\pm 30^\circ$ angleply plate—unit transverse load at $(\xi, \eta) = (70, 70)$: three-dimensional plots of (a) θ_x and (b) M_{xx} fields.

of width 0.5% of the diameter of the plate, and the Fourier series of the loading condition is given by Eq. (41) with $(\xi, \eta) = (70, 70)$. Fully clamped boundary conditions are prescribed on the circular contour. In Fig. 13(a)–(c) are shown the plots of v , w , θ_x , M_{xx} , Q_x and N_{xy} . Again, the three rows of figures from top to bottom pertain, respectively, to the particular, homogeneous and total solutions. It is observed again that the near singular behaviors in the moment and force fields are captured by the particular solu-

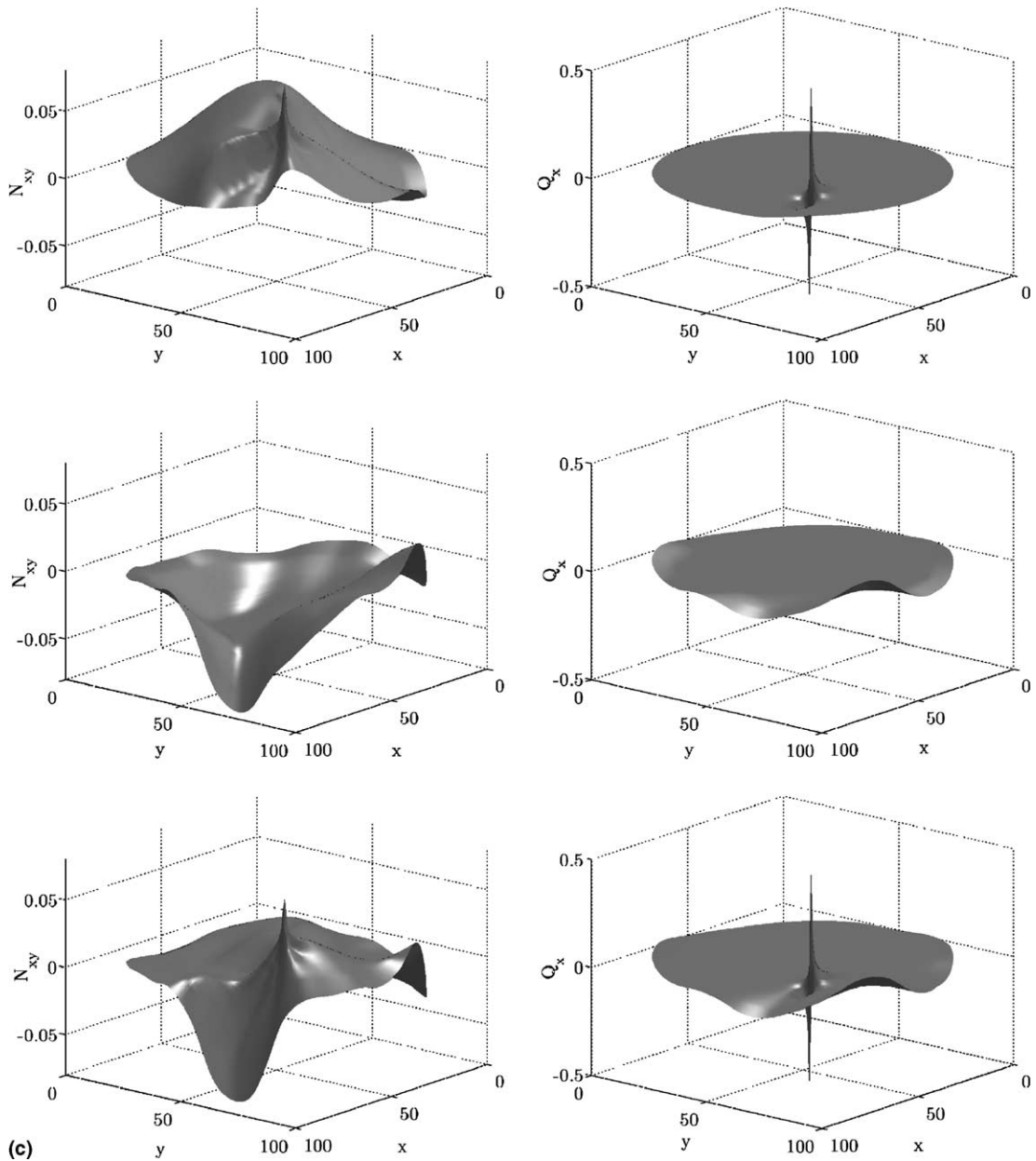


Fig. 13. (c) Circular two-layer $\pm 30^\circ$ angleply plate—unit transverse load at $(\xi, \eta) = (70, 70)$: three-dimensional plots of (a) Q_x and (b) N_{xy} .

tion, where 150^2 terms were sufficient for convergence. The homogeneous solution that meets the augmented boundary conditions was found with numerical ease using the node layout shown in Fig. 9(b) and a 2.5 normalized support. In Fig. 13(c), the coupling due to B_{16} and B_{26} resulting in N_{xy} is clearly seen.

8. Concluding remarks

An extended meshfree method was presented for the analysis of a general laminated anisotropic plate under elastostatic transverse and inplane loading. The general strategy of this method is to have the particular solution, i.e., the behavior due to loading, represented analytically by *generalized Navier* solutions and have the homogeneous solution determined by a meshfree analysis. The behavior of the particular solution on the plate's boundary go into forming the augmented boundary conditions which the homogeneous solution must meet. Thus, the sum of these two portions gives the total solution to the originally posed plate problem.

Concentrated loads on rectangular plates were considered, where these singular sources were represented by uniform loads over a very small patch. The convergence properties relating to the treatment of these nearly singular sources were explored in some detail. As this type of loads constitutes the most demanding in terms of convergence of the *generalized Navier* series representation, then all forms of distributed loading conditions can be handled as they will involve less strident representational requirements. A further example of a circular two-layer $\pm 30^\circ$ angleply plate was given to illustrate powerful features of this extended meshfree method. It can be seen that this proposed method will enable the analysis of a very large class of plate bending and two-dimensional plane stress (as well as plane strain) problems where any loading conditions, especially those involving near singularities, pose no difficulties.

Appendix A

The operators in Eq. (5) are given by

$$\begin{aligned}
 L_{11}(\cdot) &= A_{11}(\cdot)_{,xx} + 2A_{16}(\cdot)_{,xy} + A_{66}(\cdot)_{,yy} \\
 L_{12}(\cdot) &= A_{16}(\cdot)_{,xx} + (A_{12} + A_{66})(\cdot)_{,xy} + A_{26}(\cdot)_{,yy} \\
 L_{14}(\cdot) &= B_{11}(\cdot) + 2B_{16}(\cdot)_{,xy} + B_{66}(\cdot)_{,yy} \\
 L_{15}(\cdot) &= B_{16}(\cdot)_{,xx} + (B_{12} + B_{66})(\cdot)_{,xy} + B_{26}(\cdot)_{,yy} \\
 L_{22}(\cdot) &= A_{66}(\cdot)_{,xx} + 2A_{26}(\cdot)_{,xy} + A_{22}(\cdot)_{,yy} \\
 L_{24}(\cdot) &= B_{16}(\cdot) + (B_{12} + B_{66})(\cdot)_{,xy} + B_{26}(\cdot)_{,yy} \\
 L_{25}(\cdot) &= B_{66}(\cdot)_{,xx} + 2B_{26}(\cdot)_{,xy} + B_{22}(\cdot)_{,yy} \\
 L_{33}(\cdot) &= -\Gamma_{55}(\cdot)_{,xx} - 2\Gamma_{45}(\cdot)_{,xy} - \Gamma_{44}(\cdot)_{,yy} \\
 L_{34}(\cdot) &= -\Gamma_{55}(\cdot)_{,x} - \Gamma_{45}(\cdot)_{,y}, \quad L_{35}(\cdot) = -\Gamma_{45}(\cdot)_{,xx} - \Gamma_{44}(\cdot)_{,y} \\
 L_{44}(\cdot) &= D_{11}(\cdot)_{,xx} + 2D_{16}(\cdot)_{,xy} + D_{66}(\cdot)_{,yy} - \Gamma_{55}(\cdot) \\
 L_{45}(\cdot) &= D_{16}(\cdot)_{,xx} + (D_{12} + D_{66})(\cdot)_{,xy} + D_{26}(\cdot)_{,yy} - \Gamma_{45}(\cdot) \\
 L_{55}(\cdot) &= D_{66}(\cdot)_{,xx} + 2D_{26}(\cdot)_{,xy} + D_{22}(\cdot)_{,yy} - \Gamma_{44}(\cdot)
 \end{aligned} \tag{A.1}$$

Substitution of solution forms (12) and (15) into governing equations (5) leads to the following two systems of ten equations, where the upper and lower plus/minus signs, respectively, are used for the two kinematic coefficients (in bracket { , }) of the dependent variables.

$$\begin{aligned}
 (A_{11}\alpha_m^2 + A_{66}\beta_n^2)\{U_{1mn}, U_{3mn}\} \pm (A_{12} + A_{66})\alpha_m\beta_n\{V_{1mn}, V_{3mn}\} \pm 2B_{16}\alpha_m\beta_n\{\theta_{x1mn}, \theta_{x3mn}\} \\
 + (B_{16}\alpha_m^2 + B_{26}\beta_n^2)\{\theta_{y1mn}, \theta_{y3mn}\} \pm 2A_{16}\alpha_m\beta_n\{U_{2mn}, U_{4mn}\} + (A_{16}\alpha_m^2 + A_{26}\beta_n^2)\{V_{2mn}, V_{4mn}\} \\
 + (B_{11}\alpha_m^2 + B_{66}\beta_n^2)\{\theta_{x2mn}, \theta_{x4mn}\} \pm (B_{12} + B_{66})\alpha_m\beta_n\{\theta_{y2mn}, \theta_{y4mn}\} = \{0, p_{xmn}\}
 \end{aligned} \tag{A.2}$$

$$\begin{aligned} & \pm (A_{12} + A_{66})\alpha_m\beta_n\{U_{1mn}, U_{3mn}\} + (A_{66}\alpha_m^2 + A_{22}\beta_n^2)\{V_{1mn}, V_{3mn}\} + (B_{16}\alpha_m^2 + B_{26}\beta_n^2)\{\theta_{x1mn}, \theta_{x3mn}\} \\ & \pm 2B_{26}\alpha_m\beta_n\{\theta_{y1mn}, \theta_{y3mn}\} + (A_{16}\alpha_m^2 + A_{26}\beta_n^2)\{U_{2mn}, U_{4mn}\} \pm 2A_{26}\alpha_m\beta_n\{V_{2mn}, V_{4mn}\} \\ & \pm (B_{12} + B_{66})\alpha_m\beta_n\{\theta_{x2mn}, \theta_{x4mn}\} + (B_{66}\alpha_m^2 + B_{22}\beta_n^2)\{\theta_{y2mn}, \theta_{y4mn}\} = \{0, 0\} \end{aligned} \quad (\text{A.3})$$

$$\begin{aligned} & (\Gamma_{55}\alpha_m^2 + \Gamma_{44}\beta_n^2)\{W_{1mn}, W_{3mn}\} + \Gamma_{55}\alpha_m\{\theta_{x1mn}, \theta_{x3mn}\} \pm \Gamma_{44}\beta_n\{\theta_{y1mn}, \theta_{y3mn}\} \\ & \mp 2\Gamma_{45}\alpha_m\beta_n\{W_{2mn}, W_{4mn}\} \pm \Gamma_{45}\beta_n\{\theta_{x2mn}, \theta_{x4mn}\} + \Gamma_{45}\alpha_m\{\theta_{y2mn}, \theta_{y4mn}\} = \{q_{mn}, 0\} \end{aligned} \quad (\text{A.4})$$

$$\begin{aligned} & \pm 2B_{16}\alpha_m\beta_n\{U_{1mn}, U_{3mn}\} + (B_{16}\alpha_m^2 + B_{26}\beta_n^2)\{V_{1mn}, V_{3mn}\} + \Gamma_{55}\alpha_m\{W_{1mn}, W_{3mn}\} \\ & + (D_{11}\alpha_m^2 + D_{66}\beta_n^2 + \Gamma_{55})\{\theta_{x1mn}, \theta_{x3mn}\} \pm (D_{12} + D_{66})\alpha_m\beta_n\{\theta_{y1mn}, \theta_{y3mn}\} \\ & + (B_{11}\alpha_m^2 + B_{66}\beta_n^2)\{U_{2mn}, U_{4mn}\} \pm (B_{12} + B_{66})\alpha_m\beta_n\{V_{2mn}, V_{4mn}\} \mp \Gamma_{45}\beta_n\{W_{2mn}, W_{4mn}\} \\ & \pm 2D_{16}\alpha_m\beta_n\{\theta_{x2mn}, \theta_{x4mn}\} + (D_{16}\alpha_m^2 + D_{26}\beta_n^2 + \Gamma_{45})\{\theta_{y2mn}, \theta_{y4mn}\} = \{0, 0\} \end{aligned} \quad (\text{A.5})$$

$$\begin{aligned} & (B_{16}\alpha_m^2 + B_{26}\beta_n^2)\{U_{1mn}, U_{3mn}\} \pm 2B_{26}\alpha_m\beta_n\{V_{1mn}, V_{3mn}\} \pm \Gamma_{44}\beta_n\{W_{1mn}, W_{3mn}\} \\ & \pm (D_{12} + D_{66})\alpha_m\beta_n\{\theta_{x1mn}, \theta_{x3mn}\} + (D_{66}\alpha_m^2 + D_{22}\beta_n^2 + \Gamma_{44})\{\theta_{y1mn}, \theta_{y3mn}\} \\ & \pm (B_{12} + B_{66})\alpha_m\beta_n\{U_{2mn}, U_{4mn}\} + (B_{66}\alpha_m^2 + B_{22}\beta_n^2)\{V_{2mn}, V_{4mn}\} - \Gamma_{45}\alpha_m\{W_{2mn}, W_{4mn}\} \\ & + (D_{16}\alpha_m^2 + D_{26}\beta_n^2 + \Gamma_{45})\{\theta_{x2mn}, \theta_{x4mn}\} \pm 2D_{26}\alpha_m\beta_n\{\theta_{y2mn}, \theta_{y4mn}\} = \{0, 0\} \end{aligned} \quad (\text{A.6})$$

$$\begin{aligned} & \pm 2A_{16}\alpha_m\beta_n\{U_{1mn}, U_{3mn}\} + (A_{16}\alpha_m^2 + A_{26}\beta_n^2)\{V_{1mn}, V_{3mn}\} + (B_{11}\alpha_m^2 + B_{66}\beta_n^2)\{\theta_{x1mn}, \theta_{x3mn}\} \\ & \pm (B_{12} + B_{66})\alpha_m\beta_n\{\theta_{y1mn}, \theta_{y3mn}\} + (A_{11}\alpha_m^2 + A_{66}\beta_n^2)\{U_{2mn}, U_{4mn}\} \pm (A_{12} + A_{66})\alpha_m\beta_n\{V_{2mn}, V_{4mn}\} \\ & \pm 2B_{16}\alpha_m\beta_n\{\theta_{x2mn}, \theta_{x4mn}\} + (B_{16}\alpha_m^2 + B_{26}\beta_n^2)\{\theta_{y2mn}, \theta_{y4mn}\} = \{0, 0\} \end{aligned} \quad (\text{A.7})$$

$$\begin{aligned} & (A_{16}\alpha_m^2 + A_{26}\beta_n^2)\{U_{1mn}, U_{3mn}\} \pm 2A_{26}\alpha_m\beta_n\{V_{1mn}, V_{3mn}\} \pm (B_{12} + B_{66})\alpha_m\beta_n\{\theta_{x1mn}, \theta_{x3mn}\} \\ & + (B_{66}\alpha_m^2 + B_{22}\beta_n^2)\{\theta_{y1mn}, \theta_{y3mn}\} \pm (A_{12} + A_{66})\alpha_m\beta_n\{U_{2mn}, U_{4mn}\} + (A_{66}\alpha_m^2 + A_{22}\beta_n^2)\{V_{2mn}, V_{4mn}\} \\ & + (B_{16}\alpha_m^2 + B_{26}\beta_n^2)\{\theta_{x2mn}, \theta_{x4mn}\} \pm 2B_{26}\alpha_m\beta_n\{\theta_{y2mn}, \theta_{y4mn}\} = \{0, p_{ymn}\} \end{aligned} \quad (\text{A.8})$$

$$\begin{aligned} & \mp 2\Gamma_{45}\alpha_m\beta_n\{W_{1mn}, W_{3mn}\} \mp \Gamma_{45}\beta_n\{\theta_{x1mn}, \theta_{x3mn}\} - \Gamma_{45}\alpha_m\{\theta_{y1mn}, \theta_{y3mn}\} + (\Gamma_{55}\alpha_m^2 + \Gamma_{44}\beta_n^2)\{W_{2mn}, W_{4mn}\} \\ & - \Gamma_{55}\alpha_m\{\theta_{x2mn}, \theta_{x4mn}\} \mp \Gamma_{44}\beta_n\{\theta_{y2mn}, \theta_{y4mn}\} = \{0, 0\} \end{aligned} \quad (\text{A.9})$$

$$\begin{aligned} & (B_{11}\alpha_m^2 + B_{66}\beta_n^2)\{U_{1mn}, U_{3mn}\} \pm (B_{12} + B_{66})\alpha_m\beta_n\{V_{1mn}, V_{3mn}\} \pm \Gamma_{45}\beta_n\{W_{1mn}, W_{3mn}\} \\ & \pm 2D_{16}\alpha_m\beta_n\{\theta_{x1mn}, \theta_{x3mn}\} + (D_{16}\alpha_m^2 + D_{26}\beta_n^2 + \Gamma_{45})\{\theta_{y1mn}, \theta_{y3mn}\} \pm 2B_{16}\alpha_m\beta_n\{U_{2mn}, U_{4mn}\} \\ & + (B_{16}\alpha_m^2 + B_{26}\beta_n^2)\{V_{2mn}, V_{4mn}\} - \Gamma_{55}\alpha_m\{W_{2mn}, W_{4mn}\} + (D_{11}\alpha_m^2 + D_{66}\beta_n^2 + \Gamma_{55})\{\theta_{x2mn}, \theta_{x4mn}\} \\ & \pm (D_{12} + D_{66})\alpha_m\beta_n\{\theta_{y2mn}, \theta_{y4mn}\} = \{0, 0\} \end{aligned} \quad (\text{A.10})$$

$$\begin{aligned} & \pm (B_{12} + B_{66})\alpha_m\beta_n\{U_{1mn}, U_{3mn}\} + (B_{66}\alpha_m^2 + B_{22}\beta_n^2)\{V_{1mn}, V_{3mn}\} + \Gamma_{45}\alpha_m\{W_{1mn}, W_{3mn}\} \\ & + (D_{16}\alpha_m^2 + D_{26}\beta_n^2 + \Gamma_{45})\{\theta_{x1mn}, \theta_{x3mn}\} \pm 2D_{26}\alpha_m\beta_n\{U_{2mn}, U_{4mn}\} + (B_{16}\alpha_m^2 + B_{26}\beta_n^2)\{U_{2mn}, U_{4mn}\} \\ & \pm 2B_{26}\alpha_m\beta_n\{V_{2mn}, V_{4mn}\} \mp \Gamma_{44}\beta_n\{W_{2mn}, W_{4mn}\} \pm (D_{12} + D_{66})\alpha_m\beta_n\{\theta_{x2mn}, \theta_{x4mn}\} \\ & + (D_{66}\alpha_m^2 + D_{22}\beta_n^2 + \Gamma_{44})\{\theta_{y2mn}, \theta_{y4mn}\} = \{0, 0\} \end{aligned} \quad (\text{A.11})$$

The expressions for the inplane strains, changes of curvature and twist and transverse shear angles with this solution form are

$$\begin{aligned}
\varepsilon_{xx} &= \frac{\partial u}{\partial x} = \sum_m \sum_n \left[U_{1mn} \alpha_m \cos \alpha_m x \cos \beta_n y - U_{2mn} \alpha_m \sin \alpha_m x \sin \beta_n y \right. \\
&\quad \left. U_{3mn} \alpha_m \cos \alpha_m x \sin \beta_n y - U_{4mn} \alpha_m \sin \alpha_m x \cos \beta_n y \right] \\
\varepsilon_{yy} &= \frac{\partial v}{\partial y} = \sum_m \sum_n \left[V_{1mn} \beta_n \cos \alpha_m x \cos \beta_n y - V_{2mn} \beta_n \sin \alpha_m x \sin \beta_n y \right. \\
&\quad \left. -V_{3mn} \beta_n \cos \alpha_m x \sin \beta_n y + V_{4mn} \beta_n \sin \alpha_m x \cos \beta_n y \right] \\
\gamma_{xy} &= \frac{\partial u}{\partial y} + \frac{\partial v}{\partial x} = \sum_m \sum_n \left[(-U_{1mn} \beta_n - V_{1mn} \alpha_m) \sin \alpha_m x \sin \beta_n y + (U_{2mn} \beta_n + V_{2mn} \alpha_m) \cos \alpha_m x \cos \beta_n y \right. \\
&\quad \left. (U_{3mn} \beta_n - V_{3mn} \alpha_m) \sin \alpha_m x \cos \beta_n y + (-U_{4mn} \beta_n + V_{4mn} \alpha_m) \cos \alpha_m x \sin \beta_n y \right]
\end{aligned} \tag{A.12}$$

$$\begin{aligned}
\kappa_{xx} &= \frac{\partial \theta_x}{\partial x} = \sum_m \sum_n \left[-\theta_{x1mn} \alpha_m \sin \alpha_m x \sin \beta_n y + \theta_{x2mn} \alpha_m \cos \alpha_m x \cos \beta_n y \right. \\
&\quad \left. -\theta_{x3mn} \alpha_m \sin \alpha_m x \cos \beta_n y + \theta_{x4mn} \alpha_m \cos \alpha_m x \sin \beta_n y \right] \\
\kappa_{yy} &= \frac{\partial \theta_y}{\partial y} = \sum_m \sum_n \left[-\theta_{y1mn} \beta_n \sin \alpha_m x \sin \beta_n y + \theta_{y2mn} \beta_n \cos \alpha_m x \cos \beta_n y \right. \\
&\quad \left. \theta_{y3mn} \beta_n \sin \alpha_m x \cos \beta_n y - \theta_{y4mn} \beta_n \cos \alpha_m x \sin \beta_n y \right] \\
2\kappa_{xy} &= \frac{\partial \theta_x}{\partial y} + \frac{\partial \theta_y}{\partial x} = \sum_m \sum_n \left[(\theta_{x1mn} \beta_n + \theta_{y1mn} \alpha_m) \cos \alpha_m x \cos \beta_n y - (\theta_{x2mn} \beta_n + \theta_{y2mn} \alpha_m) \sin \alpha_m x \sin \beta_n y \right. \\
&\quad \left. (-\theta_{x3mn} \beta_n + \theta_{y3mn} \alpha_m) \cos \alpha_m x \sin \beta_n y + (\theta_{x4mn} \beta_n - \theta_{y4mn} \alpha_m) \sin \alpha_m x \cos \beta_n y \right]
\end{aligned} \tag{A.13}$$

$$\begin{aligned}
\gamma_{xz} &= \frac{\partial w}{\partial x} + \theta_x = \sum_m \sum_n \left[(W_{1mn} \alpha_m + \theta_{x1mn}) \cos \alpha_m x \sin \beta_n y + (-W_{2mn} \alpha_m + \theta_{x2mn}) \sin \alpha_m x \cos \beta_n y \right. \\
&\quad \left. (W_{3mn} \alpha_m + \theta_{x3mn}) \cos \alpha_m x \cos \beta_n y + (-W_{4mn} \alpha_m + \theta_{x4mn}) \sin \alpha_m x \sin \beta_n y \right] \\
\gamma_{yz} &= w_{,x} + \theta_y = \sum_m \sum_n \left[(W_{1mn} \beta_n + \theta_{y1mn}) \sin \alpha_m x \cos \beta_n y + (-W_{2mn} \beta_n + \theta_{y2mn}) \cos \alpha_m x \sin \beta_n y \right. \\
&\quad \left. (-W_{3mn} \beta_n + \theta_{y3mn}) \sin \alpha_m x \sin \beta_n y + (W_{4mn} \beta_n + \theta_{y4mn}) \cos \alpha_m x \cos \beta_n y \right]
\end{aligned} \tag{A.14}$$

References

- Becker, W., 1991. A complex potential method for plate problems with bending extension coupling. *Arch. Appl. Mech.* 61, 318–326.
- Becker, W., 1992. Closed-form analytical solution for a Griffith crack in a non-symmetric laminate plate. *Comput. Struct.* 21, 49–55.
- Becker, W., 1993. Complex method for the elliptical hole in an unsymmetric laminate. *Arch. Appl. Mech.* 63, 159–169.
- Becker, W., 1995. Concentrated forces and moments on laminates with bending extension coupling. *Comput. Struct.* 30, 1–11.
- Belytschko, T., Lu, Y.Y., Gu, L., 1994. Element-free Galerkin methods. *Int. J. Numer. Methods Eng.* 37, 256–299.
- Chen, J.S., Wu, C.T., Yoon, S., You, Y., 2001. A Stabilized conforming nodal integration for Galerkin meshfree methods. *Int. J. Numer. Methods Eng.* 50, 435–466.
- Chen, J.S., Wu, C.T., Yoon, S., 2002. Nonlinear version of stabilized conforming nodal integration for Galerkin meshfree methods. *Int. J. Numer. Methods Eng.* 53, 2587–2615.
- Chen, J.S., Wang, D.D., Dong, S.B., 2004. An extended meshfree method for boundary value problems. *Comput. Methods Appl. Mech. Engrg.* 193, 1085–1103.
- Cheng, Z.Q., Reddy, J.N., 2002. Octet formalism for Kirchhoff anisotropic plates. *Proc. Royal Soc. Lond. Ser. A* 458, 1499–1517.
- Cheng, Z.Q., Reddy, J.N., 2003. Green's functions for infinite and semi-infinite anisotropic thin plates. *J. Appl. Mech.* 70 (2), 260–267.
- Dong, S.B., Chun, C.K., 1992. Shear constitutive relations for laminated anisotropic shells and plates: part I – methodology. *J. Appl. Mech.* 59 (2), 372–379.
- Dong, S.B., Tso, F.K.W., 1972. On a laminated orthotropic shell theory including transverse shear deformation. *J. Appl. Mech.* 39 (4), 1091–1097.
- Green, A.E., Zerna, W., 1960. *Theoretical Elasticity*. Oxford University Press (see footnotes on p. 184, 185).
- Lekhnitskii, S.G., 1957. *Anisotropic Plates*. Gos. Izd., Moscow (in Russian). English Translation by Gordon and Breach, New York, 1968.
- Liu, W.K., Jun, S., Zhang, Y.F., 1995. Reproducing kernel particle methods. *Int. J. Numer. Methods Fluids* 20, 1081–1106.
- Lu, P., 1994. Stroh-type formalism for unsymmetric laminated plate. *Mech. Res. Commun.* 21, 249–254.

- Lu, P., Mahrenholtz, O., 1994. Extension of the Stroh formalism to the analysis of bending of anisotropic elastic plates. *J. Mech. Phys. Solids* 42, 1725–1741.
- Mindlin, R.D., 1951. Influence of rotatory inertia and shear on flexural motions of isotropic, elastic plates. *J. Appl. Mech.* 18, 31–38.
- Wang, D., Chen, J.S., 2004. Locking free stabilized conforming nodal integration for meshfree Mindlin–Reissner plate formulation. *Comput. Methods Appl. Mech. Engrg.* 193, 1065–1083.
- Whitney, J.M., 1987. *Structural Analysis of Laminated Anisotropic Plates*. Technomic Publishing Company, Inc., Lancaster, PA.
- Yin, W.L., 2003a. General solutions of anisotropic plates. *J. Appl. Mech.* 70 (4), 496–504.
- Yin, W.L., 2003b. Structure and properties of the solution space of general anisotropic laminates. *Int. J. Solids Struct.* 40 (8), 1825–1852.
- Zakharov, D.D., Becker, W., 2000a. Singular potentials and double-force solutions for anisotropic laminates with coupled bending and stretching. *Arch. Appl. Mech.* 70, 659–669.
- Zakharov, D.D., Becker, W., 2000b. Unsymmetric composite with a discontinuity of the in-plane displacement or of the slope. *Acta Mech.* 144, 127–135.